



HAL
open science

Strain localization in a fossilized subduction channel: Insights from the Cycladic Blueschist Unit (Syros, Greece)

Valentin Laurent, Laurent Jolivet, Vincent Roche, Romain Augier, Stéphane Scaillet, Giovanni Luca Cardello

► To cite this version:

Valentin Laurent, Laurent Jolivet, Vincent Roche, Romain Augier, Stéphane Scaillet, et al.. Strain localization in a fossilized subduction channel: Insights from the Cycladic Blueschist Unit (Syros, Greece). *Tectonophysics*, 2016, 672-673, pp.150-169. 10.1016/j.tecto.2016.01.036 . insu-01290748

HAL Id: insu-01290748

<https://insu.hal.science/insu-01290748v1>

Submitted on 18 Mar 2016

HAL is a multi-disciplinary open access archive for the deposit and dissemination of scientific research documents, whether they are published or not. The documents may come from teaching and research institutions in France or abroad, or from public or private research centers.

L'archive ouverte pluridisciplinaire **HAL**, est destinée au dépôt et à la diffusion de documents scientifiques de niveau recherche, publiés ou non, émanant des établissements d'enseignement et de recherche français ou étrangers, des laboratoires publics ou privés.



Distributed under a Creative Commons Attribution - NonCommercial - NoDerivatives 4.0 International License

1 Strain localization in a fossilized subduction channel: insights from
2 the Cycladic Blueschist Unit (Syros, Greece)

3

4 Valentin LAURENT^{1,2,3}, Laurent JOLIVET^{1,2,3}, Vincent ROCHE^{1,2,3}, Romain AUGIER^{1,2,3},
5 Stéphane SCAILLET^{1,2,3}, Giovanni Luca CARDELLO^{1,2,3}

6

7 ¹Université d'Orléans, ISTO, UMR 7327, 45071, Orléans, France

8 ²CNRS/INSU, ISTO, UMR 7327, 45071 Orléans, France

9 ³BRGM, ISTO, UMR 7327, BP 36009, 45060 Orléans, France

10 valentin.laurent@univ-orleans.fr (corresponding author), laurent.jolivet@univ-orleans.fr,
11 v.roche@brgm.fr, romain.augier@univ-orleans.fr, sscaille@cnrs-orleans.fr, luca.cardello@univ-
12 orleans.fr
13

14 Abstract:

15

16 Syros Island is worldwide known for its preservation of HP-LT parageneses in the
17 Cycladic Blueschist Unit (CBU) providing one of the best case-studies to understand the
18 tectonometamorphic evolution of a subduction channel. Conflicting structural interpretations
19 have been proposed to explain the geological architecture of Syros, in part reflecting a lack of
20 consensus about the tectonic structure of the CBU. In this study, the geological and
21 tectonometamorphic maps of Syros have been entirely redrawn in order to decipher the
22 structure of a fossilized subduction channel. Based on structural and petrological observations,
23 the CBU has been subdivided into three subunits separated by major ductile shear zones. New
24 observations of the Vari Unit confirm that it rests on top of the CBU through a detachment or
25 exhumation fault. While retrograde top-to-the E/NE shearing overprinting prograde

26 deformation is widespread across the island, the prograde deformation has been only locally
27 preserved within the less retrograded units. We show that after the prograde top-to-the S/SW
28 shearing deformation, the CBU was exhumed by an overall top-to-the E/NE shearing from the
29 depth of the eclogite-facies all the way to the depth of the greenschist-facies and finally, to the
30 brittle crust. The exhumation process encompassed the syn-orogenic stage (contemporaneous
31 of subduction, within the subduction channel - Eocene) to the post-orogenic stage
32 (contemporaneous with the formation of the Aegean Sea - Oligocene to Miocene). From syn-
33 orogenic to post-orogenic exhumation, deformation progressively localized toward the base of
34 the CBU, along large-scale ductile shear zones, allowing the preservation of earlier HP-LT
35 structures and HP-LT metamorphic parageneses. Finally, this study brings new insights on the
36 tectonometamorphic evolution of a subduction channel showing how strain localizes during
37 the history of an accretionary complex, both during the prograde and retrograde history.

38

39 Keywords

40 Subduction channel; High-pressure low-temperature metamorphism; Strain localization;
41 Ductile shear zone; Cycladic Blueschist Unit; Syros Island

42

43 Highlights

- 44 1) New geological and tectonometamorphic maps of Syros (Cyclades, Greece)
- 45 2) The Cycladic Blueschist Unit (CBU) was exhumed by an overall top-to-the east shearing
- 46 3) The CBU was exhumed as separate subunits with distinct P-T evolutions
- 47 4) Exhumation process encompassed syn- to post-orogenic stage
- 48 5) During exhumation, strain localized downward along major extensional shear zones

49

50

51 1) Introduction

52

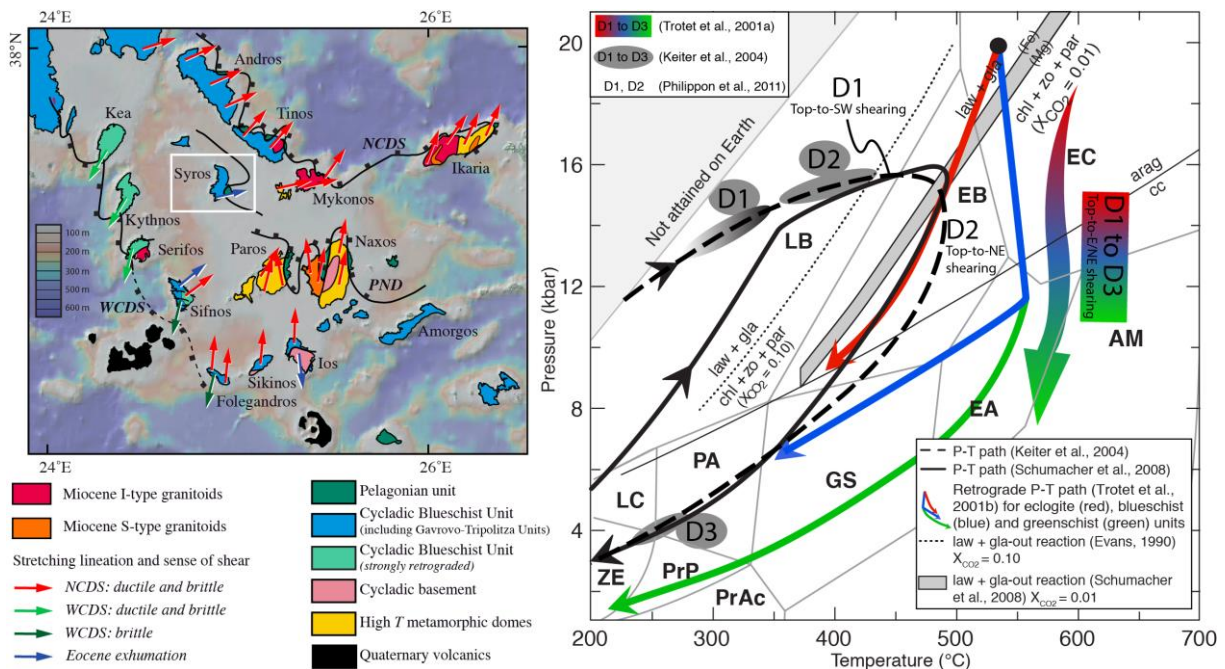
53 High-pressure low-temperature (HP-LT) metamorphic rocks are generally attributed to
54 former subduction zones. Intense retrograde deformation often overprints the early prograde
55 events, but in some key-areas, the prograde and metamorphic peak deformation can provide
56 insights on the tectonometamorphic history of a subduction zone (Alpine Corsica: [Brunet et](#)
57 [al., 2000](#); [Vitale-Brovarone et al., 2011](#); Norwegian Caledonides: [Austrheim and Griffin,](#)
58 [1985](#); [Andersen et al., 1994](#); [Labrousse et al., 2004](#); [Terry and Heidelbach, 2006](#); [Raimbourg](#)
59 [et al., 2005](#); Himalaya: [Burg et al., 1983](#); [Liou et al., 2004](#); [Epard and Steck, 2008](#); New
60 Caledonia: [Bell and Brothers, 1985](#); Aegean domain: [Keiter et al., 2004, 2011](#); [Philippon et al.,](#)
61 [2011](#)).

62 The Aegean domain and specifically the Cyclades Archipelago, form a natural
63 laboratory for studying a former subduction zone. Syros Island, located in the central part of
64 the Cyclades (Fig. 1a), is worldwide known for its spectacular preservation of deformed HP-
65 LT metamorphic rocks such as eclogites and is considered to be the type locality of
66 glaucophane ([Hausmann, 1845](#)). Rocks of this island have been the focus of many
67 petrological, geochronological and structural studies, leading to different interpretations
68 regarding: 1) the overall geometry of the CBU, 2) metamorphic peak conditions and 3) the
69 role of major tectonic contacts (Fig. 1b; [Trotet et al., 2001a, 2001b](#); [Rosenbaum et al., 2002](#);
70 [Ring et al., 2003](#); [Keiter et al., 2004, 2011](#); [Schumacher et al., 2008](#); [Philippon et al., 2011](#);
71 [Soukis and Stöckli, 2013](#)). Despite excellent outcropping conditions, these differences are
72 sometimes drastic, thus hindering our understanding of this classical example of a fossilized
73 subduction channel.

74 This paper focuses on the tectonometamorphic evolution of the Cycladic Blueschist
75 Unit. New maps and profiles are here further discussed in terms of their situation within the

76 subduction channel. We demonstrate a progressive top-to-the E/NE continuum of deformation
 77 from eclogite- to greenschist-facies. Most of the deformation completely overprinted the
 78 prograde subduction-related deformation. However, we highlight areas where syn-burial
 79 tectonometamorphic features are preserved. In addition, we confirm the existence of the Vari
 80 Detachment recently challenged by Philippon et al. (2011) as an extensional detachment
 81 partly responsible for the exhumation of the CBU. Finally, deep-seated subduction processes
 82 are then discussed in the framework of the Hellenic subduction zone.

83



84
 85 Figure 1: Localization of the studied area and Pressure-Temperature-deformation paths of Syros available in
 86 literature. a) Tectonic map of the Cyclades showing the major tectonic structures such as the North Cycladic
 87 Detachment System (NCDS), the West Cycladic Detachment System (WCDS) and the Paros-Naxos Detachment
 88 (PND), as well as kinematic indicators, after Jolivet et al. (2015). b) Representation of the different calculated P-
 89 T paths for the CBU in Syros. D1, D2 and D3 phases of deformation after Trotet et al. (2001a, 2001b), Keiter et
 90 al. (2004), Philippon et al. (2011) highlight the conflicting prograde or retrograde interpretations of the main
 91 deformation observed on Syros. Facies: AM, amphibolite; EA, epidote-amphibolite; EB, epidote-blueschist; EC,
 92 eclogite; GS, greenschist; LB, lawsonite-blueschist; LC, lawsonite-chlorite; PA, pumpellyite-actinolite; PrAc,
 93 prehnite-actinolite; PrP, prehnite-pumpellyite; ZE, zeolite (after Peacock, 1993). Lawsonite + glaucophane-out
 94 reactions after Evans (1990) and Schumacher et al. (2008).
 95

96

97

98

99 2) Geological setting

100

101 2.1) Tectonometamorphic evolution of the Cycladic Blueschist Unit

102

103 The Aegean domain, part of the eastern Mediterranean Sea, experienced a two steps
104 tectonometamorphic evolution. Firstly, the late Cretaceous-Eocene formation of the
105 Hellenides-Taurides chain resulted from the subduction and collision of the Apulian
106 microcontinent with Eurasia (Bonneau and Kienast, 1982; Dercourt et al., 1986; van
107 Hinsbergen et al., 2005). The entrance of the Apulian crust in the subduction zone led to an
108 episode of crustal thickening and syn-orogenic exhumation of HP-LT metamorphic units such
109 as the Cycladic Blueschist Unit (CBU; Fig. 1a; Blake et al., 1981; Bonneau and Kienast, 1982;
110 Jolivet et al., 2003, 2004; Brun and Faccenna, 2008; Jolivet and Brun, 2010; Ring et al., 2010).
111 Secondly, post-orogenic extension in the Rhodope from 45 Ma and in the Aegean Sea from
112 35 Ma was associated with the retreat of the African slab (Jolivet and Faccenna, 2000; Brun
113 and Sokoutis, 2010; Jolivet and Brun, 2010; Ring et al., 2010). In the Aegean domain, part of
114 western Anatolia and in the Rhodope Massif, back-arc extension of the previously thickened
115 crust was accommodated by several regional-scale detachments such as the North Cycladic
116 Detachment System (NCDS) or the West Cycladic Detachment System (WCDS) (Fig. 1a;
117 Jolivet et al., 2010; Grasemann et al., 2012).

118 Located in the center of the Aegean domain, the Cyclades correspond to the deepest
119 exhumed parts of the Hellenides-Taurides chain and are mainly composed by the CBU (Fig.
120 1a). This unit is mainly made of marbles, metapelites and metabasites all showing peak P-T
121 conditions in the blueschist- or eclogite-facies (Blake et al., 1981; Bonneau, 1984; Okrush and
122 Bröcker, 1990; Avigad and Garfunkel, 1991; Trotet et al., 2001b; Schumacher et al., 2008).
123 The CBU experienced alpine tectonic and metamorphic evolution, with an early burial in HP-

124 LT conditions reaching ~18-20 kbar and 500-550 °C (Fig. 1b; Dürr et al., 1978; Bröcker and
125 Enders, 2001; Trotet et al., 2001b; Parra et al., 2002; Tomaschek et al., 2003; Augier et al.,
126 2015) during the Eocene (~50-35 Ma; Tomaschek et al., 2003; Putlitz et al., 2005; Lagos et al.,
127 2007). During the Oligocene and for the whole Miocene, this event was followed by LP-HT
128 greenschist- to amphibolite-facies overprint of variable intensity (Fig. 1a; Altherr et al., 1979,
129 1982; Wijbrans and McDougall, 1986; Buick, 1991; Keay et al., 2001; Vanderhaeghe, 2004;
130 Duchêne et al., 2006; Bröcker et al., 2013; Beaudoin et al., 2015). On top of the CBU, the
131 Upper Cycladic Unit (UCU) corresponds to the uppermost parts of the nappe stack. The UCU
132 is composed of Permian to Mesozoic metasediments, minor orthogneisses and ophiolites
133 equilibrated in greenschist- to amphibolite-facies metamorphic conditions during the
134 Cretaceous, sometimes covered with Oligocene to Miocene sediments (Sanchez-Gomez et al.,
135 2002; Kuhlemann et al., 2004; Lecomte et al., 2010; Menant et al., 2013). Structurally below
136 the CBU, the Cycladic Continental Basement (CCB) crops out as large-scale tectonic
137 windows on several islands in the central and southern part of the Cyclades (Fig. 1a; e.g.
138 Paros, Naxos, Ios or Sikinos; Andriessen et al., 1987). This unit is composed of Variscan
139 orthogneisses enveloped by metasediments that locally retain metamorphic relics of
140 amphibolite-facies assemblages suggesting a complex pre-alpine history (Bonneau and
141 Kienast, 1982; Andriessen et al., 1987; Keay, 1998; Photiades and Keay, 2003; Gupta and
142 Bickle, 2004; Huet et al., 2009; Augier et al., 2015). Late exhumation stages of both the CBU
143 and the CCB were accompanied by emplacement of syn-tectonic Miocene intrusions (i.e.
144 Tinos, Mykonos, Ikaria, Naxos, Serifos, Lavrio; Fig. 1a; Jansen, 1973; Altherr et al., 1982;
145 Faure et al., 1991; Lee and Lister, 1992; Altherr and Siebel, 2002; Pe-Piper et al., 2002;
146 Grasemann and Petrakakis, 2007; Iglseder et al., 2009; Bolhar et al., 2010; Lecomte et al.,
147 2010; Stouraiti et al., 2010; Denèle et al., 2011; Laurent et al., 2015; Rabillard et al., 2015).

148

149 2.2) Geology of Syros

150

151 Located in the central part of the Aegean domain, Syros is mainly composed by the
152 CBU except for the Vari Unit (Fig. 2a). Vari Unit, composed of greenschist mylonites and
153 orthogneiss, corresponds to a distinct tectonic unit attributed to UCU, separated from the CBU
154 by the Vari Detachment (Trotet et al., 2001a; Keiter et al., 2004, 2011; Soukis and Stöckli,
155 2013). The basal part of the CBU crops out in the southwestern part of the island and is
156 mainly composed of albitic micaschists and rare gneisses (e.g. the Komito gneiss; Fig. 2a;
157 Hecht, 1985). Structurally above, the central part of Syros is dominated by alternating
158 sequences of marble and micaschist layers (Fig. 2a). In this area, metabasites are a minor
159 component and often occur as dismembered boudins intercalated within the metamorphic
160 series. Conversely, in other parts of the island and especially in the north, metabasites form
161 the dominant lithology and often occur as kilometer-scale massive bodies (e.g. Hecht, 1985;
162 Keiter et al., 2004, 2011; Philippon et al., 2011). Metabasites are locally turned into massive
163 eclogite-facies rocks but also occur as blueschist- or greenschist-facies rocks (Trotet et al.,
164 2001a).

165

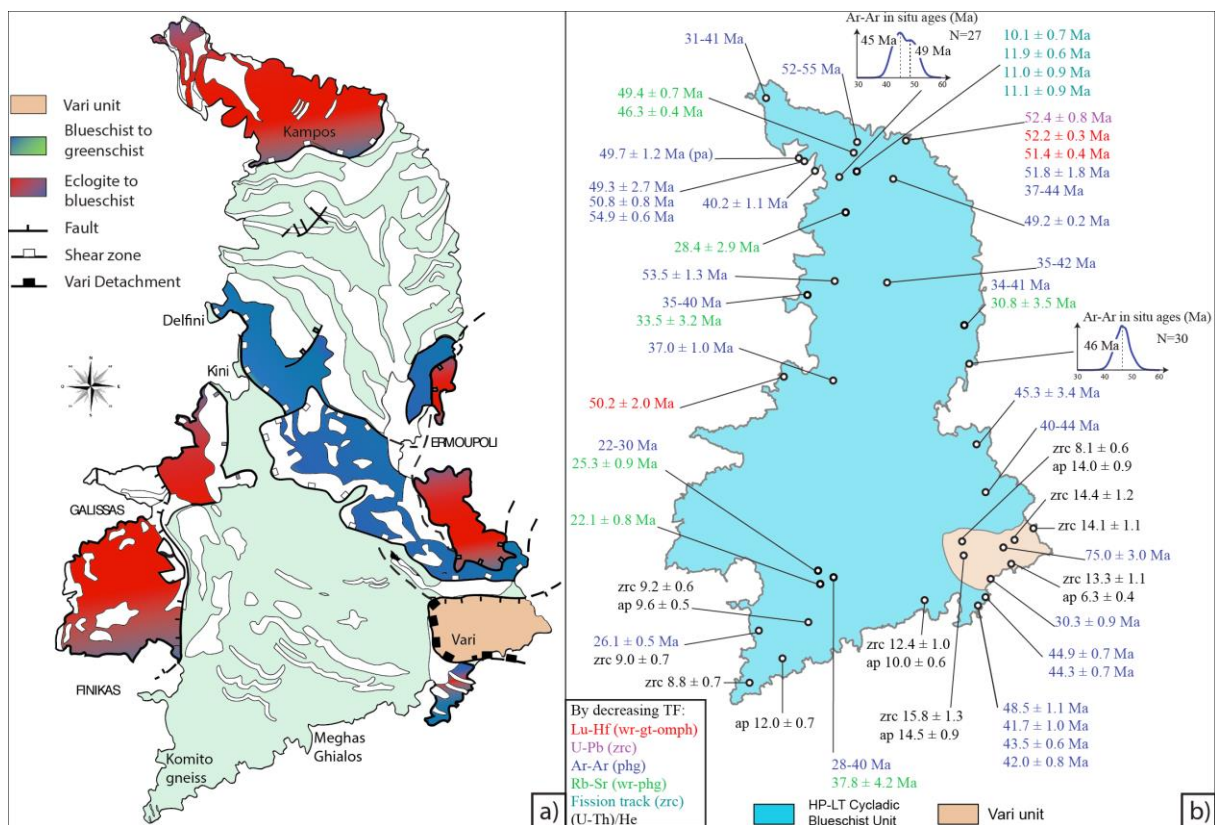
166 2.3) Pressure-Temperature-time evolution

167

168 Petrological studies yielded contrasting estimates for metamorphic peak conditions
169 from 15-16 kbar and 500°C (Schliestedt et al., 1987; Okrusch and Bröcker, 1990; Avigad and
170 Garfunkel, 1991; Schmädicke and Will, 2003; Schumacher et al., 2008) to 19-20 kbar and
171 525-550°C (Fig. 1b; Trotet et al., 2001b; Groppo et al., 2009; Dragovic et al., 2012; Ashley et
172 al., 2014). Timing and duration of this subduction-related P-T evolution have been quite well
173 constrained since the 1980s, using a large panel of isotopic systems such as K-Ar, $^{40}\text{Ar}/^{39}\text{Ar}$,

174 Rb-Sr, U-Pb, Lu-Hf, Sm-Nd systems on various minerals (Fig. 2b; Altherr et al., 1979, 1982;
 175 Andriessen et al., 1979; Wijbrans and McDougall, 1986; Maluski et al., 1987; Wijbrans et al.,
 176 1990; Bröcker et al., 1993, 2013; Bröcker and Franz, 1998, 2006; Bröcker and Enders, 1999;
 177 Tomaschek et al., 2003; Putlitz et al., 2005; Lagos et al., 2007; Huet, 2010; Dragovic et al.,
 178 2012). Studies attempting to date the burial culmination led to ca. 53-49 Ma ages (Tomaschek
 179 et al., 2003; Putlitz et al., 2005; Lagos et al., 2007). Then, the retrogression in the greenschist-
 180 facies has been dated between 25 and 21 Ma (Bröcker et al., 2013). Final exhumation stages
 181 of the CBU were recently constrained by low-temperature thermochronological tools between
 182 12 and 8 Ma (Fig. 2b; Ring et al., 2003; Soukis and Stöckli, 2013).

183



184

185 Figure 2: Previous geological and geochronological works on Syros. a) Metamorphic map of Syros showing the
 186 main tectonic structures, after Trotet et al. (2001a). b) Compilation of previous geochronological data calculated
 187 after U-Pb (Bröcker & Enders, 1999; Tomaschek, et al., 2003), Lu-Hf (Lagos, et al., 2007), ⁴⁰Ar/³⁹Ar (Maluski et
 188 al., 1987; Tomaschek, et al., 2003; Putlitz et al., 2005; Huet, 2010; Bröcker et al., 2013), Rb-Sr (Bröcker &
 189 Enders, 2001; Bröcker et al., 2013), (U-Th)/He (Soukis and Stöckli, 2013) and fission track methods (Ring et al.,
 190 2003).

191

192

193 2.4) Main controversies

194

195 The relative importance of the prograde and retrograde deformations, compression *vs*
196 extension, syn-orogenic *vs* post-orogenic exhumation is still debated. Hecht (1985) elaborated
197 the geological map of Syros at the scale 1: 50000 and interpreted all basal contacts of
198 metabasites as tectonic, mostly as thrusts, contradicting the initial interpretation of metabasite
199 occurrences as olistoliths within a flysch sequence (Bonneau et al., 1980a, 1980b; Blake et al.,
200 1981). Recently, Keiter et al. (2011) remapped the entire island at the scale 1: 25000. These
201 authors argued that an important result of their study is the identification of a significant late
202 brittle deformation on Syros that was so far poorly constrained. In parallel, Philippon et al.
203 (2011) reinterpreted the geological map of Syros, based on the original map of Hecht (1985).
204 These authors disconfirmed the existence of the Vari Detachment, correlating the Vari and
205 Komito gneisses and repositioning the Vari Unit at the base of the CBU. Soukis and Stöckli
206 (2013) challenged this conclusion, restoring the original interpretation of Gautier (1995),
207 Trotet et al. (2001a) or Ring et al. (2003), thus recognizing the juxtaposition of the Vari Unit
208 onto the CBU by the Vari Detachment. A second controversy relates to the regional and
209 tectonic significance of the deformation recorded by HP-LT rocks. According to Trotet et al.
210 (2001a), the main deformation phase is retrograde and was acquired during exhumation of the
211 CBU from eclogite- to greenschist-facies (D1 to D3; Fig. 1b). For these authors, exhumation
212 occurred during a continuum of top-to-the E/NE shearing deformation from the early Eocene
213 (syn-orogenic exhumation) to the early Miocene (post-orogenic exhumation). In contrast,
214 Keiter et al. (2004, 2011) interpreted the main deformation event affecting the CBU as
215 prograde, implying therefore a rigid body exhumation of the whole structure (D1 to D3; Fig.
216 1b). Finally, Philippon et al. (2011) describe two distinct ductile phases of deformation (Fig.

217 1b), i) a first top-to-the SW prograde deformation (D1) and, ii) a second extensional top-to-
218 the NE penetrative shear (D2) affecting the entire CBU.

219 As long as these discrepancies are not addressed, the deep processes and long-term
220 evolution of the CBU in the subduction channel will remain poorly understood.

221

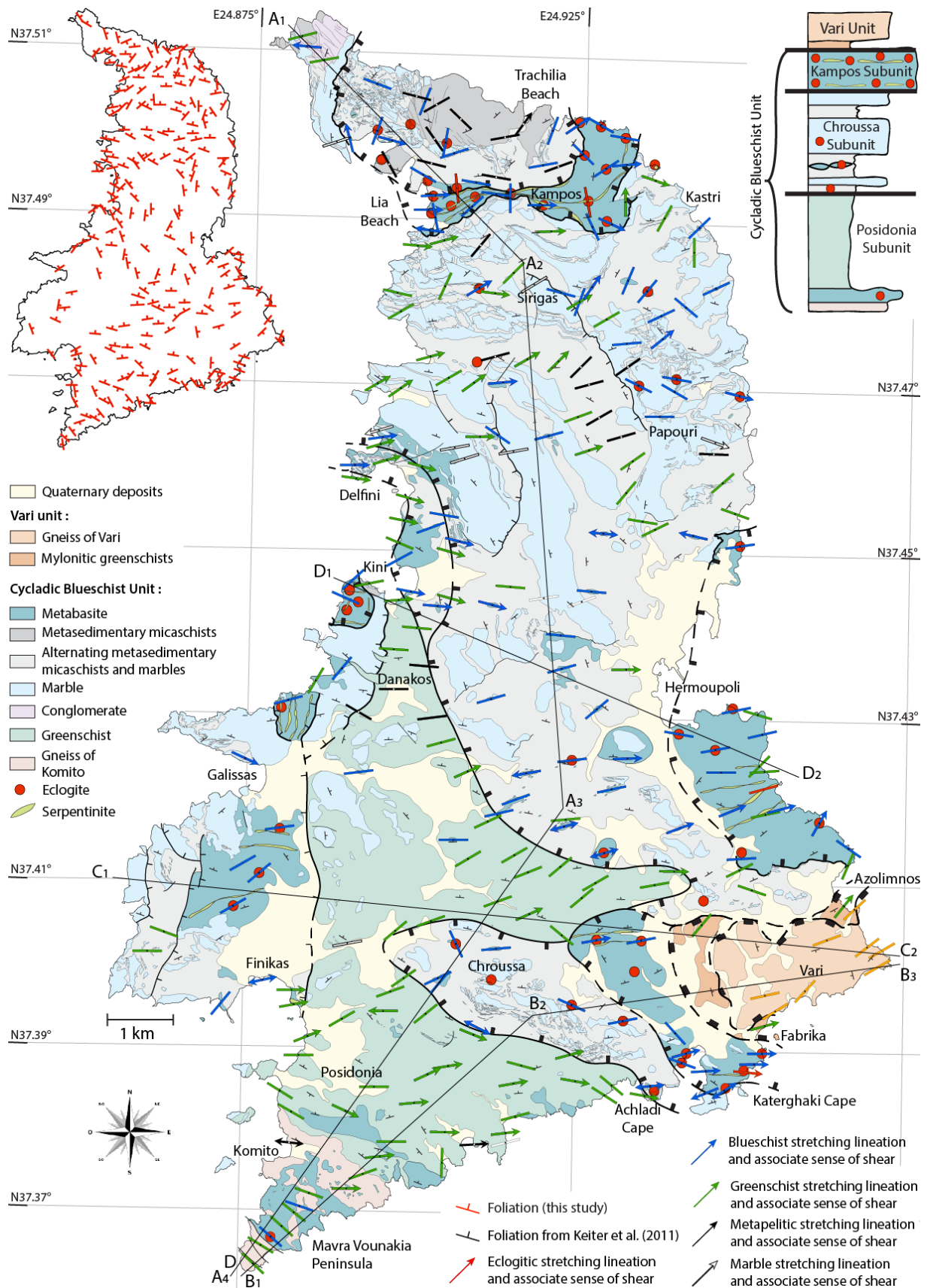
222 3) A new geological map of Syros

223

224 3.1) Method and mapping technique

225

226 In order to complement existing geological maps and put constraints on the geometry
227 of Syros, the whole island has been remapped based on field observations and satellite-images
228 interpretation (Fig. 3). Lithology and tectonic boundaries have been redrawn following our
229 observations all over the island. For mutual comparison, the color code of the legend is the
230 same as in the geological map of Keiter et al. (2011), with simplified lithologic subdivisions
231 for the purpose of our tectonometamorphic study. Calcitic and dolomitic marbles were
232 merged together into a unique metacarbonate comprehensive unit. Similarly, further
233 subdivisions within the mafic protoliths were abandoned. Anyway, principal occurrences of
234 serpentinite and eclogite are reported on the map (Fig. 3). Additionally, the finite strain
235 markers were studied as well as the link with the metamorphic record. Results are given on
236 figure 3.



237
238
239
240
241

Figure 3: New geological map of Syros showing the main tectonic structures and lithologic distributions (geometry of the Vari Unit after Soukis and Stöckli, 2013). Cross-sections are traced with black lines and highlight the architecture of Syros. Planar (foliation planes) and linear (stretching lineations) fabrics are represented with their associated metamorphic facies. Also shown are the localities cited in the text.

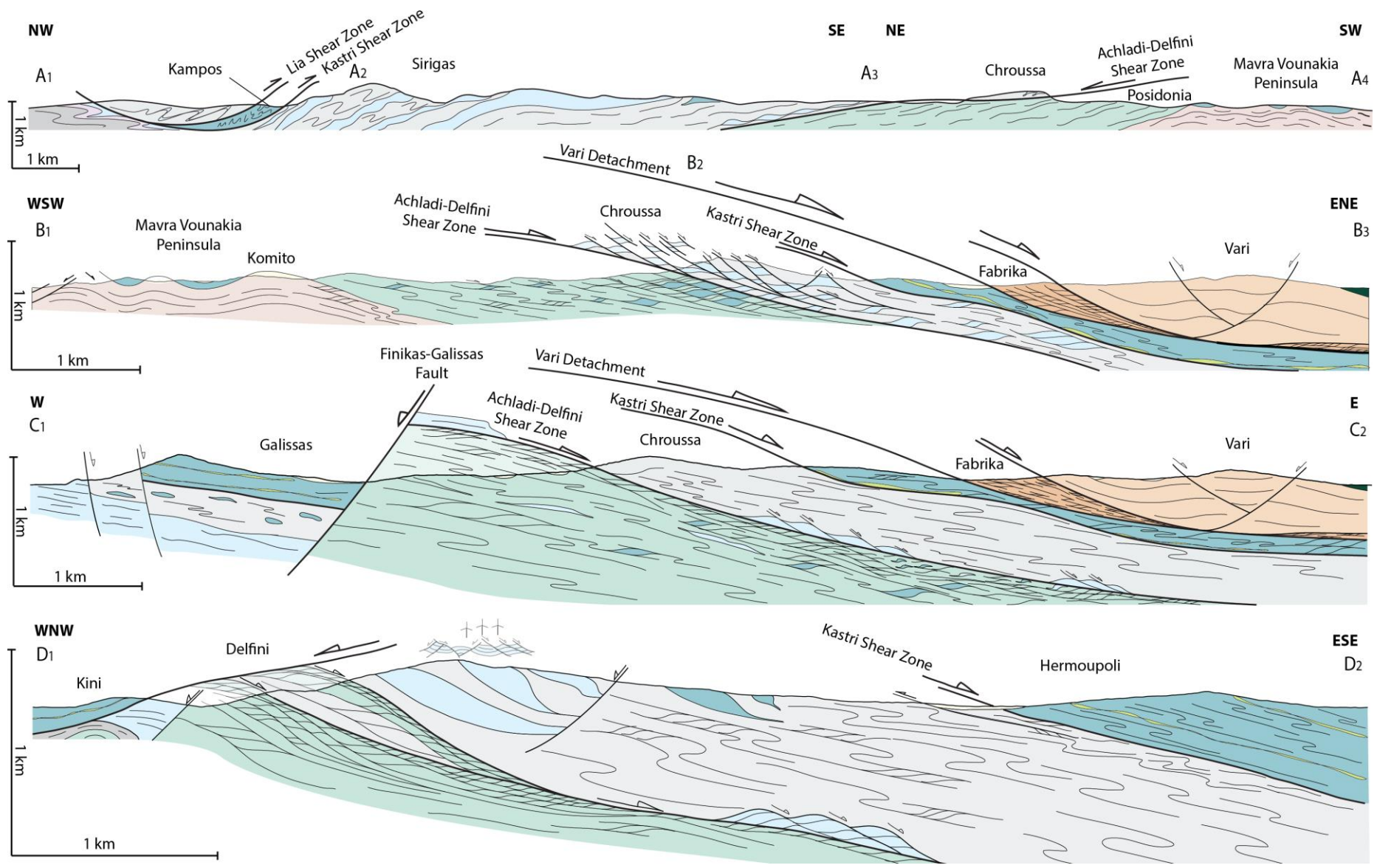


Figure 3 (continue)

242
243

244 3.2) Large-scale structure

245

246 From a lithological point of view, our new geological map does not significantly differ
247 from the one of Keiter et al. (2011) with only few areas where minor changes are reported; the
248 map thus seems relatively robust. As examples of differences, we highlight larger outcrops of
249 metabasites in several parts of the island, like in Mavra Vounakia peninsula or near the
250 Delfini Bay (Fig. 3).

251 The most obvious changes are related to the structural aspects in a broad sense, and
252 particularly the way the metamorphic sequence is structured in coherent units. Our approach
253 consisted first in the identification of high strain zones (i.e. major shear zones) where
254 deformation is concentrated, and second, in the recognition of subunits characterized by their
255 lithological content and metamorphic record. This mapping approach allows us redefining the
256 stack of the CBU, subdividing it in three subunits delimited by major shear zones, which are
257 from bottom to top:

258 1) Posidonia Subunit, which is lithologically subdivided in two parts: the structurally lower
259 felsic gneiss of Komito with intercalated boudins of metabasite, overlain by albitic
260 micaschists, few metabasites and thin marble layers (Fig. 3). The entire basal unit has been
261 overprinted in the greenschist-facies with only few areas preserving high-pressure relics in
262 centimeter-scale mafic boudins (Fig. 3). The Achladi-Delfini Shear Zone delimits the
263 Posidonia Subunit from the upper Chroussa Subunit.

264 2) Chroussa Subunit, which is composed of a lithostratigraphic sequence of alternating
265 micaschists, thick marble layers and metabasites (Fig. 3). Although some areas are more
266 overprinted in the greenschist-facies, blueschist-facies parageneses are well preserved in this
267 subunit. Fresh eclogites are sometimes preserved in the core of metabasic boudins of any
268 scale (Fig. 3). The Kastri Shear Zone delimits the Chroussa Subunit from the upper Kampos

269 Subunit.

270 3) Kampos Subunit, which is mainly composed of a mélange of metabasites, including
271 metagabbros, metabasalts, and locally still visible remains of metapillow-lavas (see [Keiter et](#)
272 [al., 2011](#) for details) wrapped by strongly foliated metapelites and/or serpentinites. Within this
273 subunit, eclogite- and blueschist-facies parageneses are preserved, with only few narrow
274 zones overprinted in the greenschist-facies (Fig. 3). The Vari Detachment delimits the top of
275 Kampos Subunit, and at larger scale the entire CBU, from the upper Vari Unit.

276 Finally, the Vari Unit is formed from bottom to top by a greenschist mylonitic unit and
277 the gneiss of Vari intruding amphibolite-facies metabasites (see also Soukis and Stöckli,
278 2013). High-pressure rocks were not recognized in the Vari Unit.

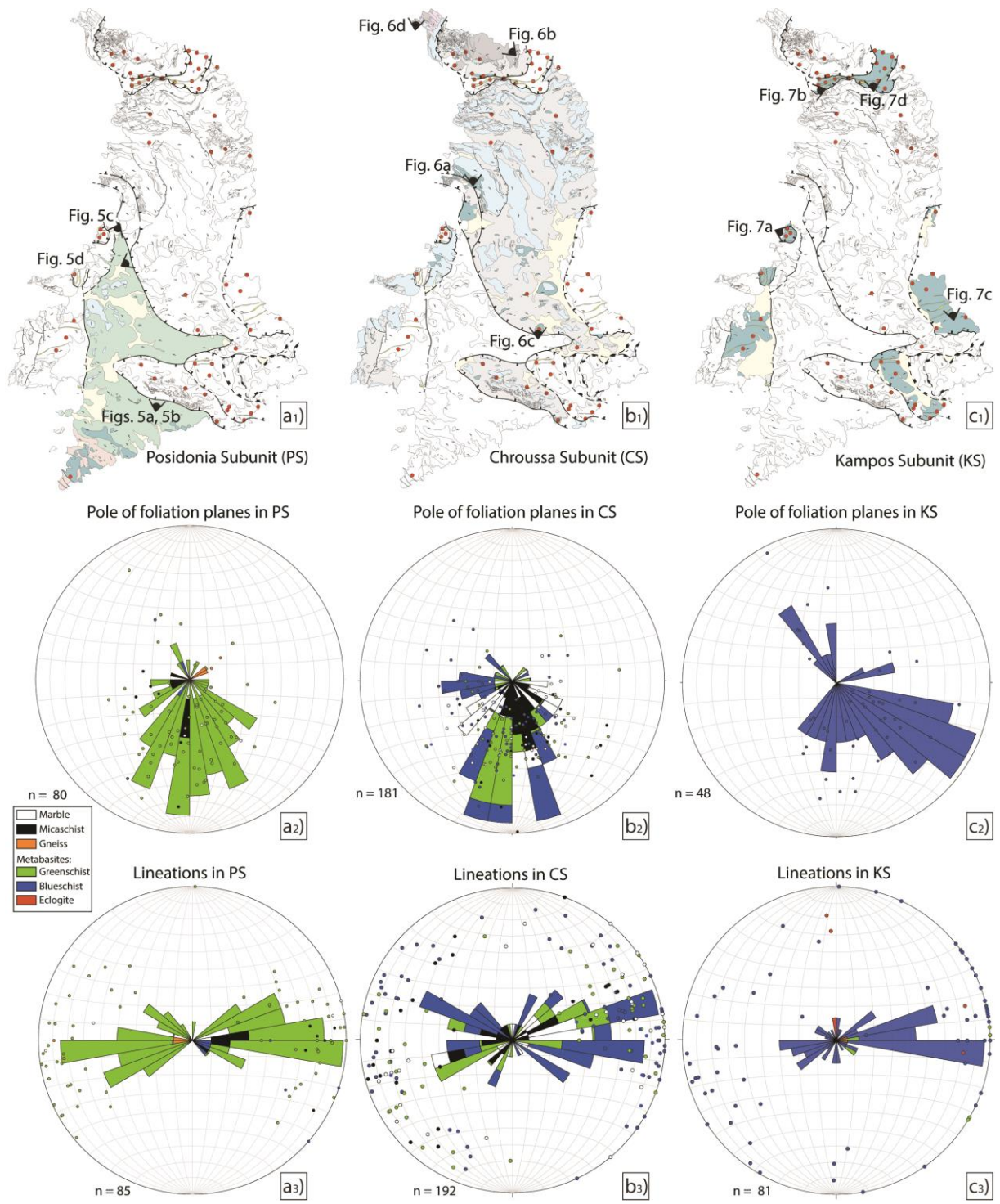
279

280 4) Deformation and metamorphic record in the CBU

281

282 Finite strain markers were studied throughout the island. In parallel, physical conditions
283 of the deformation were evaluated by the recognition of syn-kinematic minerals in
284 metabasites and other types of lithologies. All three subunits experienced HP-LT imprint in
285 the eclogite-facies conditions. This initial record is however unevenly distributed. In this
286 section we explore the relationships between the preservation/retrogression of HP-LT
287 parageneses and the relative intensity of deformation.

288



289
 290
 291
 292
 293
 294
 295
 296
 297

Figure 4: Stereograms of the planar and linear fabric measured on Syros and their associated metamorphic facies or lithology if mineralogy does not allow identifying the metamorphic-facies. a₁, b₁, c₁) Geological maps highlighting respectively the Posidonia, Chroussa and Kampos subunits and localizing the pictures displayed on the figures 5, 6 and 7. a₂, b₂, c₂) Rose diagram of the poles of foliation planes in each subunit. a₃, b₃, c₃) Rose diagram of stretching lineations in each subunit.

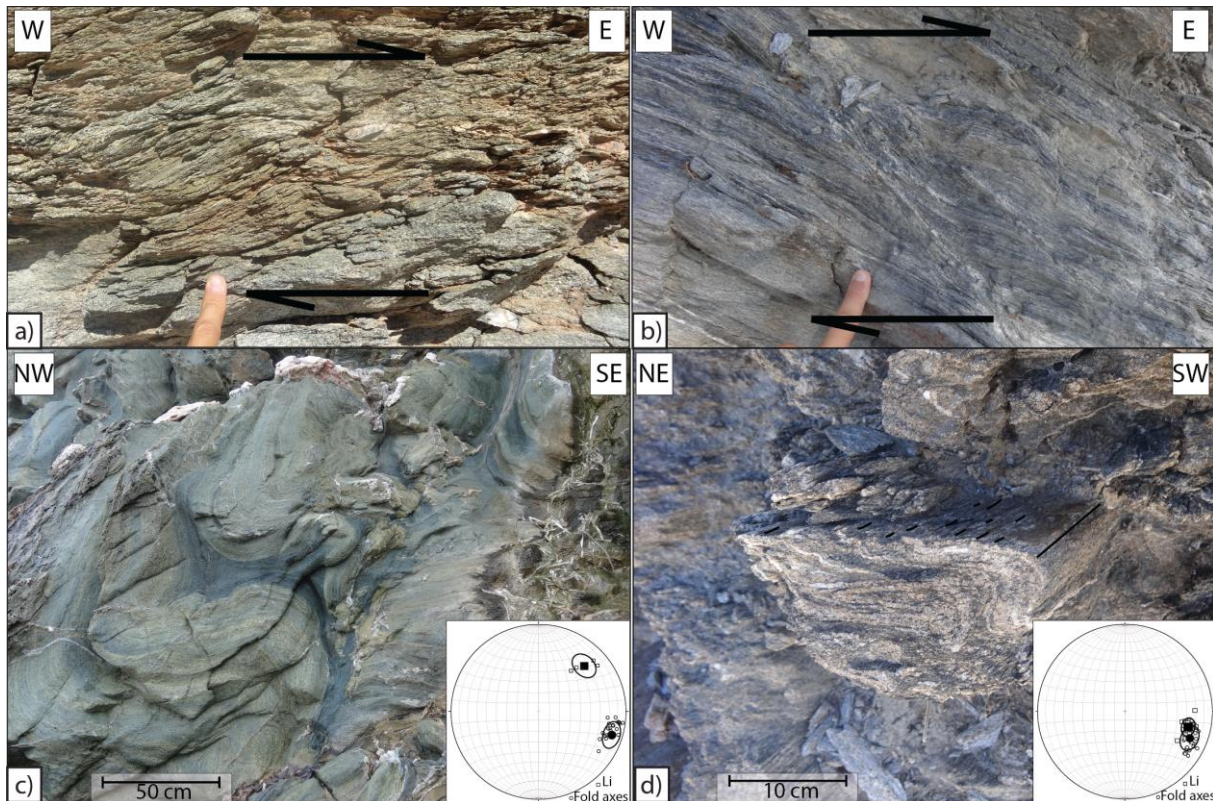
298 4.1) Posidonia Subunit

299

300 Foliation in Posidonia Subunit dips shallowly toward NNW to NNE (Fig. 4a). A syn-
301 greenschist facies stretching lineation is observed almost systematically, marked by the
302 stretching of syn-kinematic chlorite and/or albite in rocks showing only greenschist
303 parageneses (Fig. 4a). Syn-blueschist lineations were observed in only four outcrops (Fig. 3).
304 For each of these areas, HP-LT markers are preserved within up to a few meters thick mafic
305 to ultra-mafic boudins hosted in greenschist-facies rocks. The trend of stretching lineations
306 varies between N60°E to N100°E with a dominant E-W orientation (Fig. 4a). Foliation planes
307 and stretching lineations measured in the Mavra Vounakia Peninsula (Fig. 3) are slightly
308 different from those observed in the rest of Posidonia Subunit. There, foliation planes
309 measured in gneiss and metabasites are NW-SE trending with oscillating dip direction toward
310 the NE or SW and carried stretching lineations oriented between N120°E and N140°E (Fig. 3).

311 In Posidonia Subunit, markers of non-coaxial ductile deformation are observed as
312 shear bands, sigma-clast systems, drag folds or asymmetric boudinage. For more than 90% of
313 visited outcrops, these markers indicate a consistent syn-greenschist top-to-the east sense of
314 shear (Figs. 3, 5a, 5b). Additionally, the rocks of Posidonia Subunit are tightly to isoclinally
315 folded, with fold axes either parallel or perpendicular to the stretching direction (Figs. 5c, 5d).

316



317
 318 Figure 5: Syn-greenschist top-to-the east shearing characterizing the Posidonia Subunit. Localization of pictures
 319 is showing on figure 4a₁. a, b) Syn-greenschist top-to-the east shear bands (GPS coordinate: 37°23'16.2'' /
 320 24°54'21.5'') c) Greenschist folds characterized by orthogonal fold axes compared to syn-greenschist stretching
 321 lineations (GPS coordinate: 37°26'40.5'' / 24°53'53.8''). Data are plotted on the stereogram. d) Parallel fold
 322 axes and syn-greenschist stretching lineations observed in the contact zone with the Chroussa Subunit near the
 323 village of Danakos (GPS coordinate: 37°26'06'' / 24°54'05.1''). Data are plotted on lower hemisphere
 324 stereograms.

325

326 4.2) Chroussa Subunit

327

328 Chroussa Subunit consists of a succession of marble layers, micaschists and
 329 metabasites, showing both syn-blueschist and syn-greenschist deformation (Fig. 4b).
 330 Measured foliation planes shallowly dip to north (Fig. 4b) with local variations. Within
 331 blueschist-facies rocks, a group of N-S striking foliation planes dips eastward (Fig. 4b). Two
 332 other orientations of foliation planes were measured in marbles, dipping toward the NE or the
 333 NW (Fig. 4b). As for Posidonia Subunit, only a few foliation planes dip southward. The
 334 planar fabric observed in Chroussa Subunit is often associated with a stretching lineation
 335 marked by glaucophanes needles in blueschist-facies rocks and chlorite and/or albite pods in

336 greenschist-facies rocks (Fig. 4b). Overall, the bulk of measured stretching lineations shows a
337 constant orientation with a rather low dispersion between N70°E and N100°E. A subordinate
338 N20°E set of lineations is observed in blueschist-facies rocks (Fig. 4b).

339 Rocks of Chroussa Subunit are strongly deformed at all scales. Markers of non-coaxial
340 ductile deformation are similar to those observed in Posidonia Subunit. Likewise, this subunit
341 shows top-to-the E/NE ductile deformation for both syn-blueschist and syn-greenschist
342 markers (Figs. 6a, 6b, 6c). In the northern part of Syros, near Trachilia Beach, top-to-the
343 northeast shear bands affecting lawsonite pseudomorphs in metapelites occur (Fig. 6b). In few
344 places, we observed in the Chroussa Subunit shear bands or asymmetric boudinage showing
345 retrograde top-to-the west deformation (Figs. 3, 6c). Folds are also common in Chroussa
346 Subunit showing curved axes locally parallel to the stretching lineation and axial closures like
347 in sheath folds (Fig. 6d).

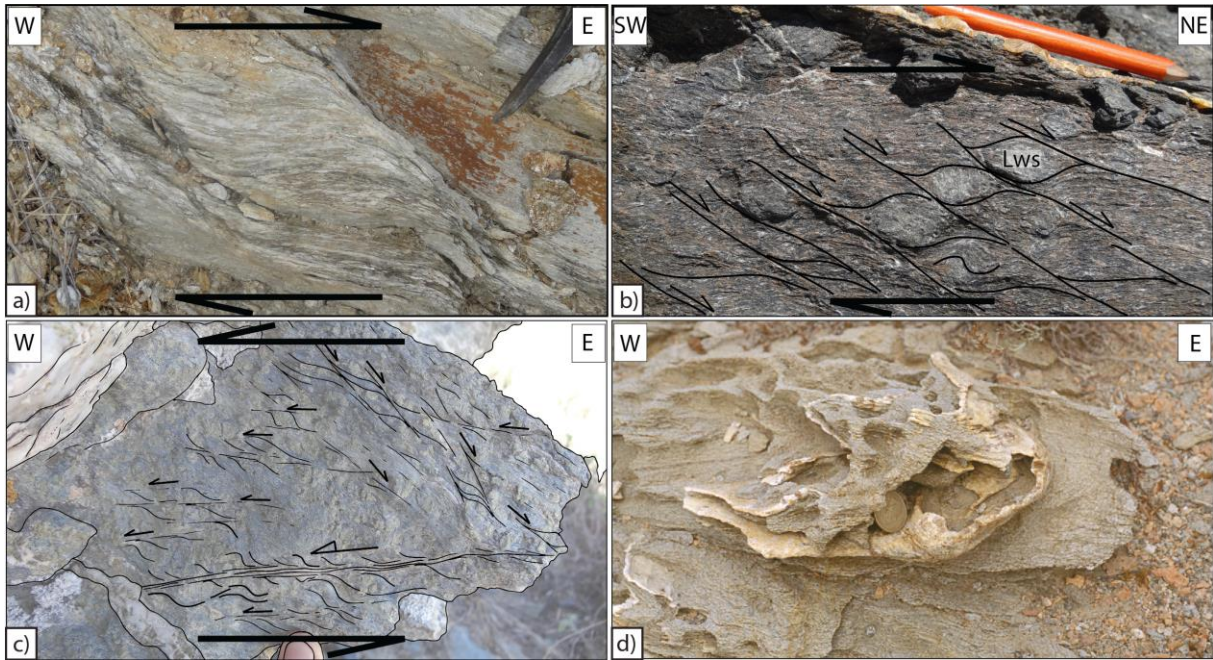
348

349

350

351

352



353
 354 Figure 6: Shearing criteria observed in Chroussa Subunit. Outcrop location is shown on figure 4a₂. a) Syn-
 355 greenschist top-to-the east shear bands (GPS coordinate: 37°28'24.1'' / 24°55'11.6''). b) Top-to-the northeast
 356 shear bands affecting preserved pseudomorphs of lawsonite (GPS coordinate: 37°30'07.9'' / 24°54'54.4''). c)
 357 Retrograde top-to-the west shearing observed locally in the Chroussa Subunit (GPS coordinate: 37°24'49.3'' /
 358 24°55'45.5''). The steep shear planes are secondary shear zones rotating top west with an antithetic sense of
 359 shear. d) Curved axis fold observed in micaschists, sub-parallel to the stretching lineation and showing closure
 360 typical of sheath fold (GPS coordinate: 37°30'39.4'' / 24°52'39.3'').

361

362

363 4.3) Kampos Subunit

364

365 Kampos Subunit displays rocks equilibrated in eclogite- and blueschist-facies.

366 Foliation planes dip toward north or northwest (Fig. 4c). Stretching lineations are mainly

367 oriented between N70°E and N100°E and dominantly marked by elongated glaucophane

368 minerals along a main stretching direction (Fig. 4c). N-S syn-blueschist stretching lineations

369 are common in the metabasites near Kampos village (Figs. 3, 4c). In some outcrops (e.g. Kini,

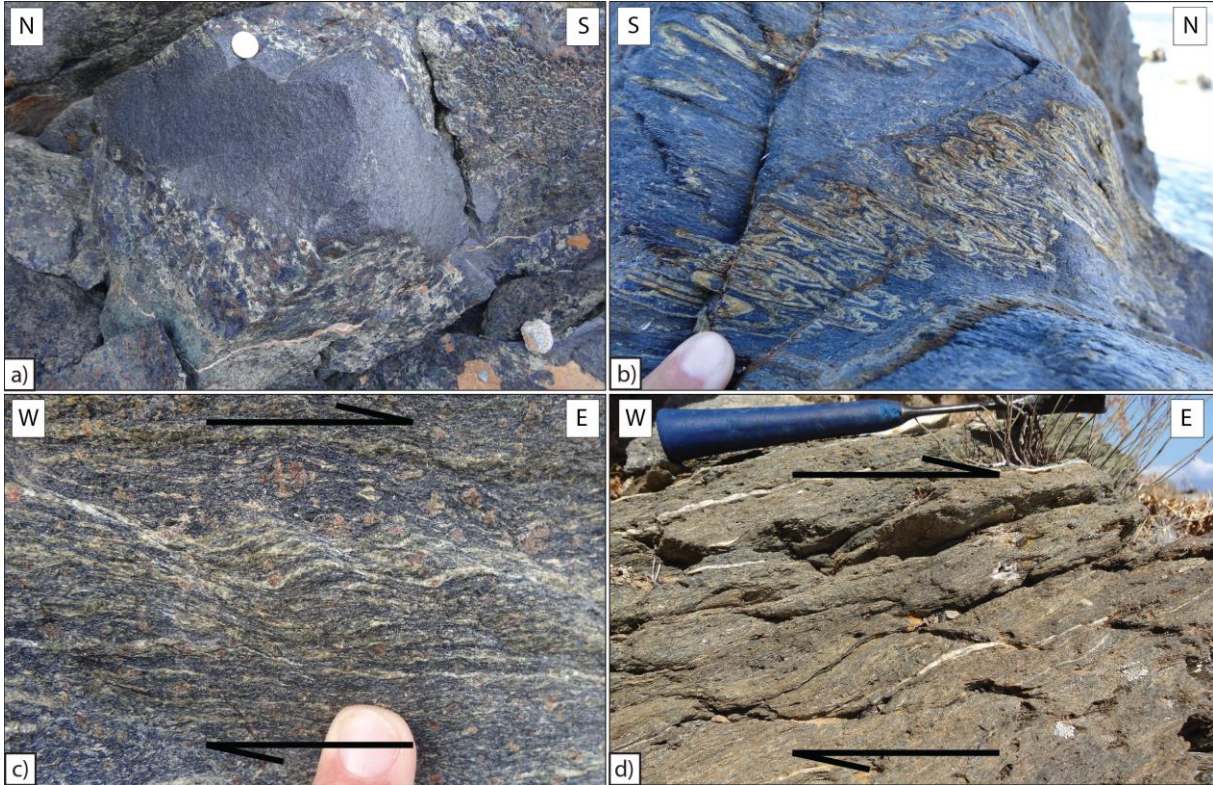
370 Kampos or near the airport), metabasite bodies show only incipient deformation with

371 preserved metapillow-lavas or metabasaltic dykes crosscutting metagabbros (Fig. 7a).

372 Conversely, in others outcrops, rocks experienced intense top-to-the-east shearing recorded

373 during retrogression of eclogites in blueschist-facies conditions (Fig. 7). This characteristic

374 top-to-the east ductile deformation increases up-section toward the contact with Vari Unit,
375 defining a single strain gradient accompanied by a gradient of eclogite retrogression.
376



377
378 Figure 7: Intense syn-eclogite to blueschist-facies deformation of Kampos Subunit illustrating top-to-the east
379 sense of shear. Localization of pictures is showing on figure 4a₃. a) Metabasaltic dyke cross-cutting a massive
380 metagabbro unit showing no deformation (GPS coordinate: 37°26'43.6'' / 24°53'20.4''). b) Isoclinal folds
381 characterized by sub-horizontal axes parallel to the stretching lineation. These folds show intense thinning during
382 shearing with pure shear component during deformation (GPS coordinate: 37°29'19.2'' / 24°54'03.4''). c, d)
383 Syn-blueschist top-to-the east shearing affecting high-pressure metabasites (GPS coordinate: c) 37°25'05.3'' /
384 24°57'42.9'' d) 37°29'22.6'' / 24°55'42.1'').

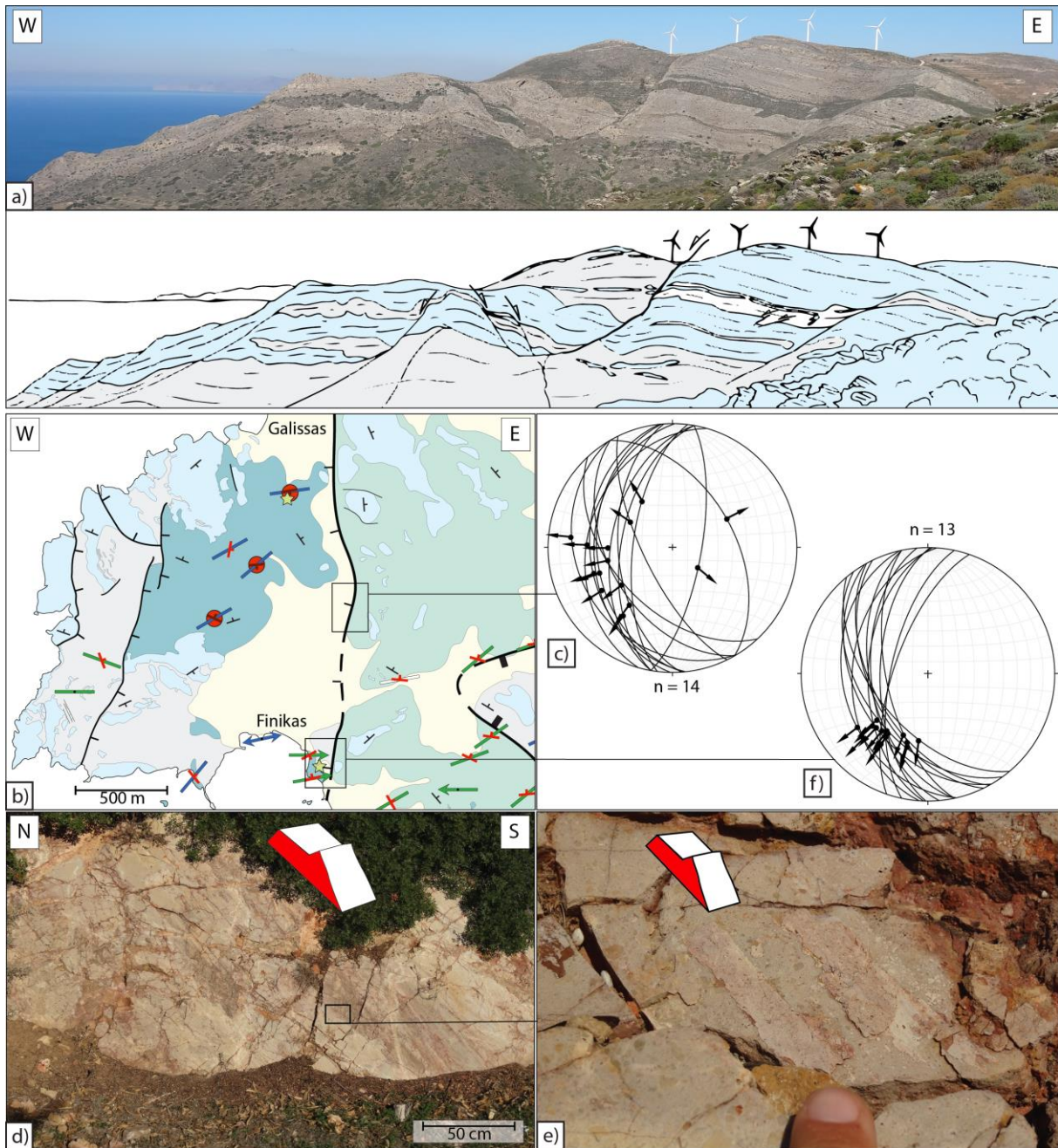
385
386

387 4.4) Brittle deformation

388

389 Ductile features are affected by late, sometime pervasive, brittle deformation recorded
390 in all units by both low and high-angle normal faults. These normal faults are well exposed
391 near Sirigas where they offset two large boudinaged marble layers (Fig. 8a). Two normal
392 faults, occurring between Sirigas and Papouri and close to Kini, reach the critical size to be
393 followed at map scale (Fig. 3). Near Galissas (see location on Fig. 8b), the strongly

394 retrogressed rocks of Posidonia Subunit are in contact with the HP-LT blueschist- and
395 eclogite-facies metabasites of Kampos Subunit (Figs. 3, 8b). Quaternary slope deposits cover
396 this contact. Along the road between Finikas and Galissas, a west-dipping fault zone with
397 cataclasites and striations crops out for about 50 m-long, showing oblique normal kinematics
398 with top-to-the W-SW sense of movement (Figs. 8b, 8c, 8d, 8e). On top of this fault plane, a
399 3-4 m-thick brittle fault gouge is observed. Moreover, south of Finikas, we observed normal
400 faults trending N-S with similar top-to-the southwest kinematics (Fig. 8b, 8f). These two
401 outcrops characterize a 4 km-long late brittle normal fault, the Finikas-Galissas Fault (Figs. 3,
402 8b).



403
 404 Figure 8: Field photographs of observed brittle normal faults. a) Panorama (Chroussa Subunit) showing coeval
 405 top-to-the east and west ductile-brittle to purely brittle normal faults. b) Zoom of the geological map showing
 406 location of outcrops along the Finikas-Galissas Fault. c) Associated stereogram showing measured brittle normal
 407 fault planes that indicate top-to-the W/SW kinematic. d) Brittle fault plane observed along the main road
 408 between Finikas and Galissas. e) Zoom on the striated fault plane showing the normal sense of motion. f)
 409 Stereogram showing brittle normal fault planes measured near Finikas village that indicate top-to-the southwest
 410 kinematic.

411

412

413

414

415

416 5) Geometry, kinematics and metamorphic conditions of the major contacts

417

418 If the Vari Detachment has already been described in previous works ([Soukis and](#)
419 [Stöckli, 2013](#)), some of the major contacts described below were so far either neglected (i.e.
420 Achladi-Delfini Shear Zone), or not fully understood in previous works. The new map,
421 supported by field data and satellite observation, allows us to identify their main
422 characteristics and role in the island overall architecture.

423

424 5.1) Posidonia-Chroussa subunits contact: the Achladi-Delfini Shear Zone

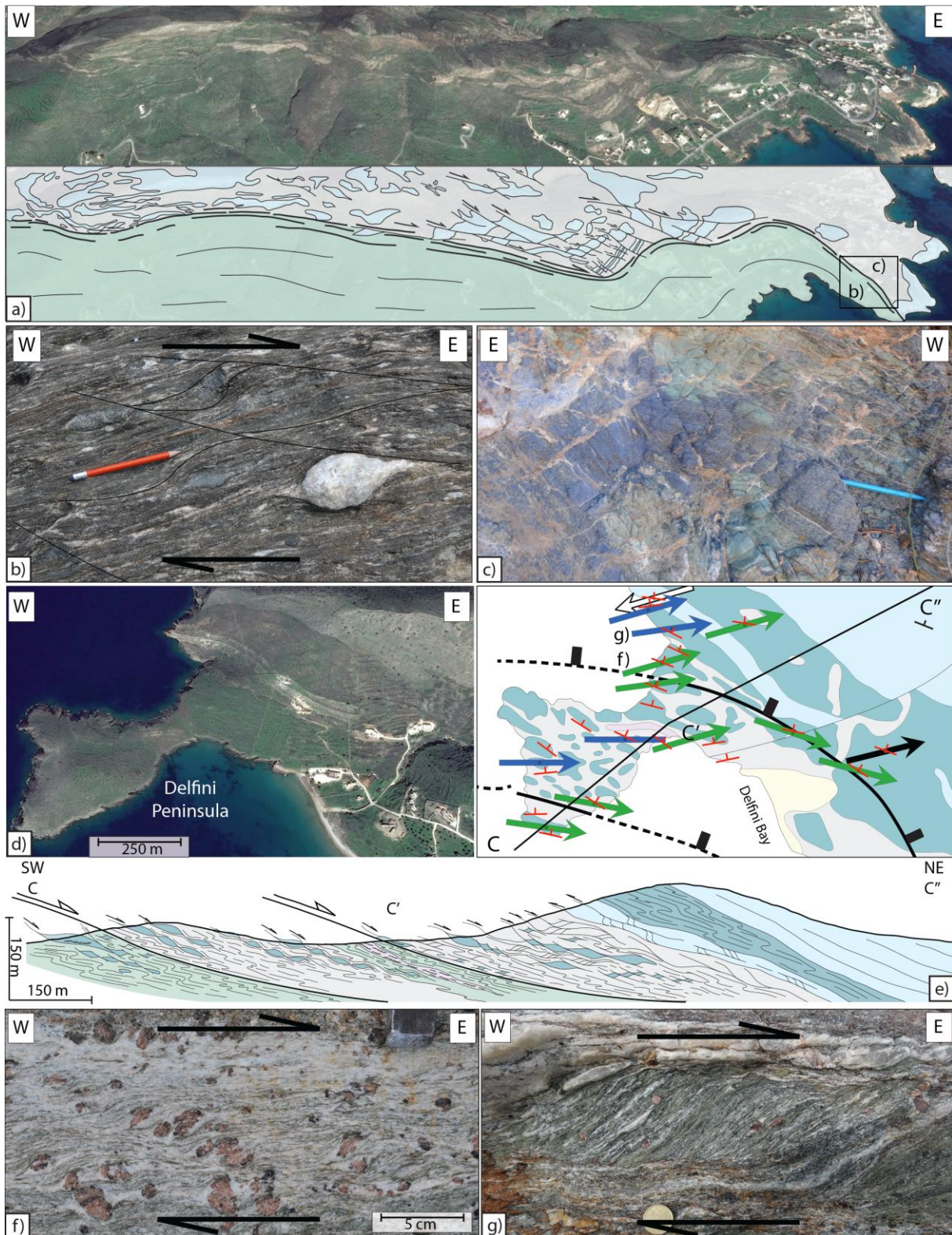
425

426 The Posidonia-Chroussa subunits contact is exposed between Achladi Cape and
427 Delfini (Fig. 9, see location on Fig. 3). In its southern limit, the trace of the shear zone can be
428 followed over more than 3 km in the landscape, shown by the non-coaxial deformation of
429 marbles layers (Fig. 9a). Some marble layers are affected by brittle normal faults, while others
430 are boudinaged and separated by ductile shear zones rooting in the contact between Chroussa
431 and Posidonia subunits. Whatever the regime of deformation and the physical conditions that
432 prevailed, ductile or brittle, clear top-to-the east deformation is observed in the form of a thick
433 shear zone (Fig. 9a). Below, the intensity of greenschist-facies retrogression increases in the
434 vicinity of the shear zone, where metabasites are turned into chlorite-albite prasinites in which
435 former HP-LT imprint is not detectable in the field. For example, west of Cape Achladi along
436 the southern coast of the island, rocks of the Posidonia Subunit are strongly overprinted by
437 greenschist-facies parageneses. At the cape, a metaconglomerate of Posidonia Subunit
438 consisting of basic and calcitic pebbles embedded in heavily retrogressed metapelitic matrix
439 crops out just below the contact. Within this metaconglomerate, pebbles are ductilely sheared
440 with a top-to-the east kinematic (Fig. 9b). Structurally a few meters above, a ca. 20 m-long

441 outcrop of preserved blueschist-facies metabasite is associated with eclogite boudins (Fig. 9c).
442 This sharp transition from well-preserved blueschists and eclogites above strongly retrograded
443 rocks below also supports the presence of a major shear zone between the Posidonia and
444 Chroussa subunits, named in this study the Achladi-Delfini Shear Zone.

445 Furthermore, the same contact between Posidonia and Chroussa subunits is exposed
446 around Delfini Bay that is bounded to the west by a small peninsula (Fig. 9d). Along a SW to
447 NE transect through Delfini peninsula, two blue- to greenschist-facies shear zones are
448 observed (Figs. 9d, 9e). Top-to-the east kinematic indicators such as shear bands, sigmoidal
449 pressure shadows on garnets or drag folds associated with crystallization of syn-kinematic
450 chlorite and albite are observed within the Delfini peninsula (Figs. 9f, 9g). These two
451 metamorphic transition zones, distant of ca. 500 m, define the contact between Posidonia and
452 Chroussa subunits. These shear zones have each accommodated a part of the total
453 displacement and can be considered at large-scale as a single structure, the Achladi-Delfini
454 Shear Zone (Fig. 3).

455 Despite poorer outcrop conditions within the island, the trace of this contact was
456 followed by combining structural and metamorphic observations, looking especially for the
457 preservation of HP-LT minerals. These field observations were strengthened by detailed
458 analysis of aerial pictures. At map-scale, the resulting geometry of the Achladi-Delfini Shear
459 Zone shows a sinuous contact extending over 13 km through the island (Fig. 3).



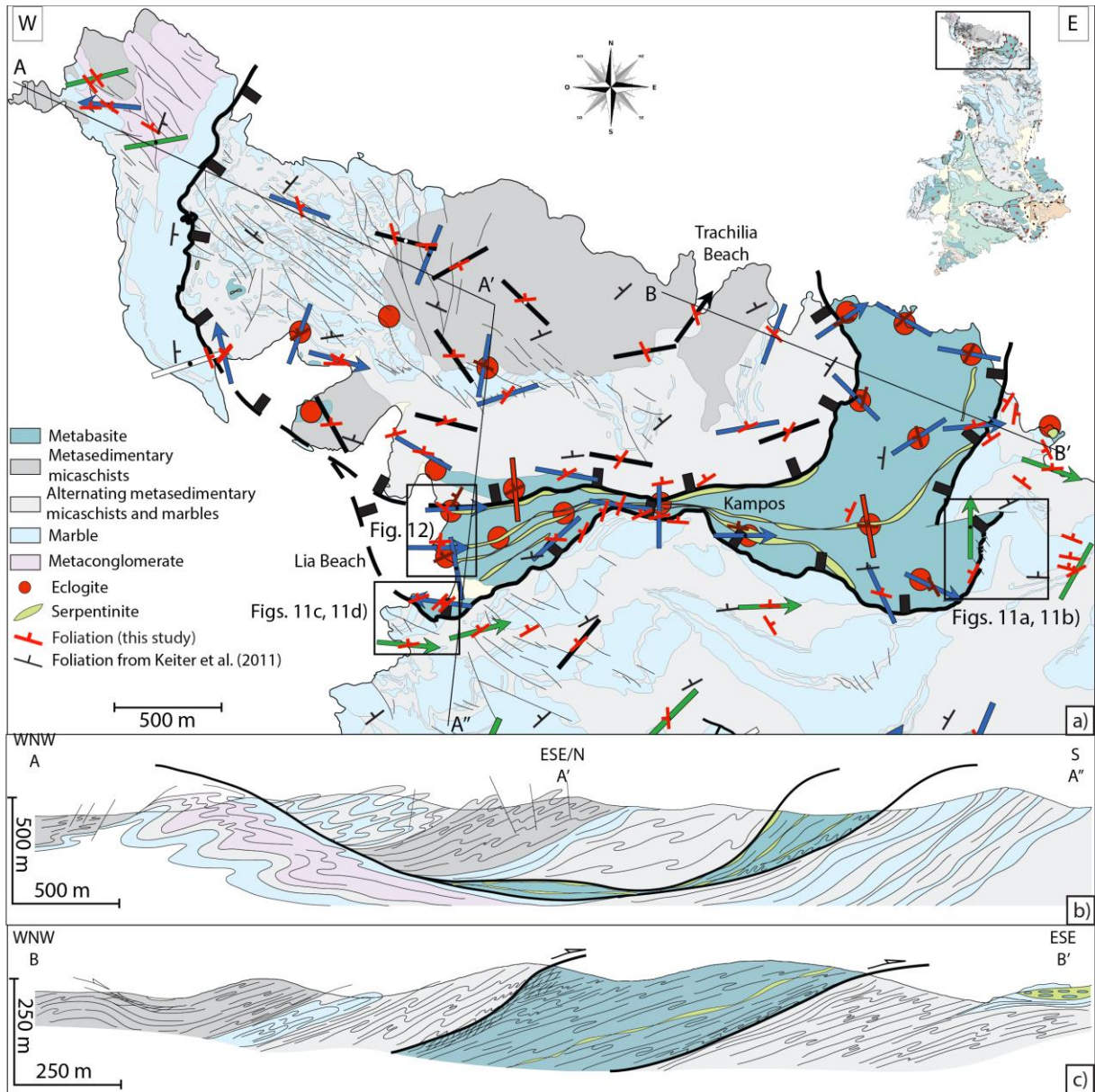
460
 461 Figure 9: The top-to-the east Achladi-Delfini Shear Zone. a) Satellital image of the Achladi-Delfini Shear Zone
 462 observed above Achladi Cape and its interpretation showing top-to-the east sense of shear. b) Top-to-the east
 463 shearing in a greenschist metaconglomerate unit located just below the contact. c) Structurally few meters above,
 464 in the Chroussa Subunit, massive glaucophanites are observed with eclogitic boudins. d) Satellital image of the
 465 Delfini peninsula and its geological interpretation. e) Geological cross-section through the Delfini peninsula
 466 illustrating the architecture of the Achladi-Delfini Shear Zone. f) Top-to-the east kinematic indicators observed
 467 in retrogressed greenschist-facies rocks. g) Syn-blueschist top-to-the east shearing observed in the Chroussa
 468 Subunit.

469 5.2) Chroussa-Kampos subunits contact: the Kastri and Lia Shear Zones

470

471 The contact between Chroussa and Kampos subunits is well exposed in the northern
472 part of the island, along the Kampos metabasite belt (Fig. 10; see also [Keiter et al., 2004,](#)
473 [2011](#)). This metabasic unit shows an E-W orientation and dips toward the north on the
474 western side. It strikes more N-S dipping westward in its eastern half (Fig. 10). The northern
475 and southern contact zones of the Kampos Subunit, i.e. the basal and roof contacts, are nicely
476 exposed along the coast, especially on the way to Lia Beach (Fig. 10).

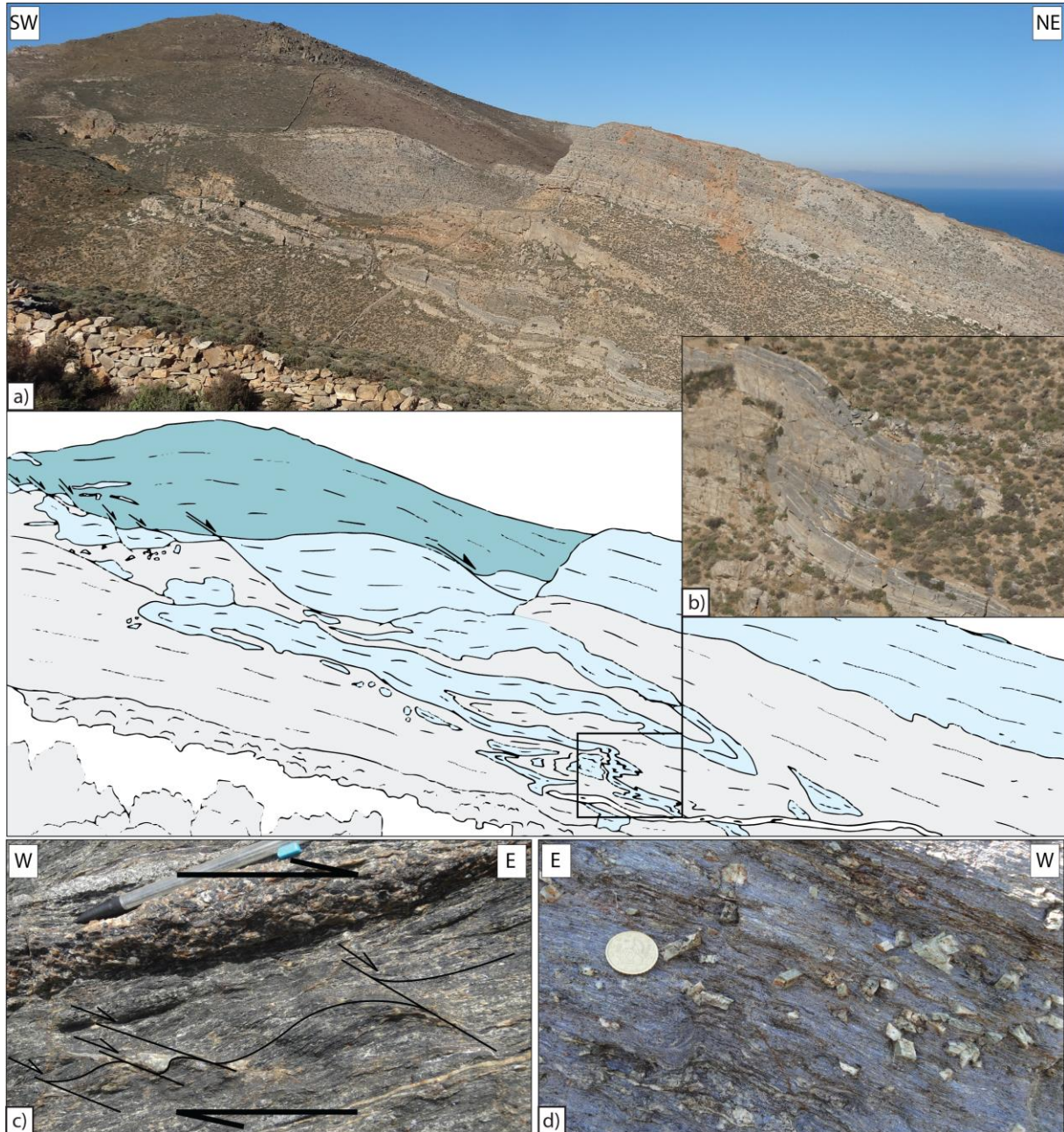
477



478
 479 Figure 10: Geological architecture of the northern part of Syros. a) Geological map showing locations of cross-
 480 sections and figures 12 and 13. b) Cross-section illustrating the organization and deformation of structures. Note
 481 that large shear zones surround the western part of the Kampos metabasite belt. c) Detailed cross-section of the
 482 eastern part of the Kampos metabasite belt.
 483
 484

485 The basal contact of Kampos Subunit with Chroussa Subunit can be seen in the
 486 landscape near Kastri (Fig. 11a). At the contact, the marble layers of Chroussa Subunit are
 487 boudinaged and sheared, some of them showing large-scale sigmoids (Fig. 11a). These
 488 structures define a large-scale top-to-the northeast shear zone, named in this study the Kastri
 489 Shear Zone. Just below the contact, tightly folded marble intercalations occur as a result of
 490 intense shearing along this major shear zone (Fig. 11b). In contrast to the Kampos Subunit

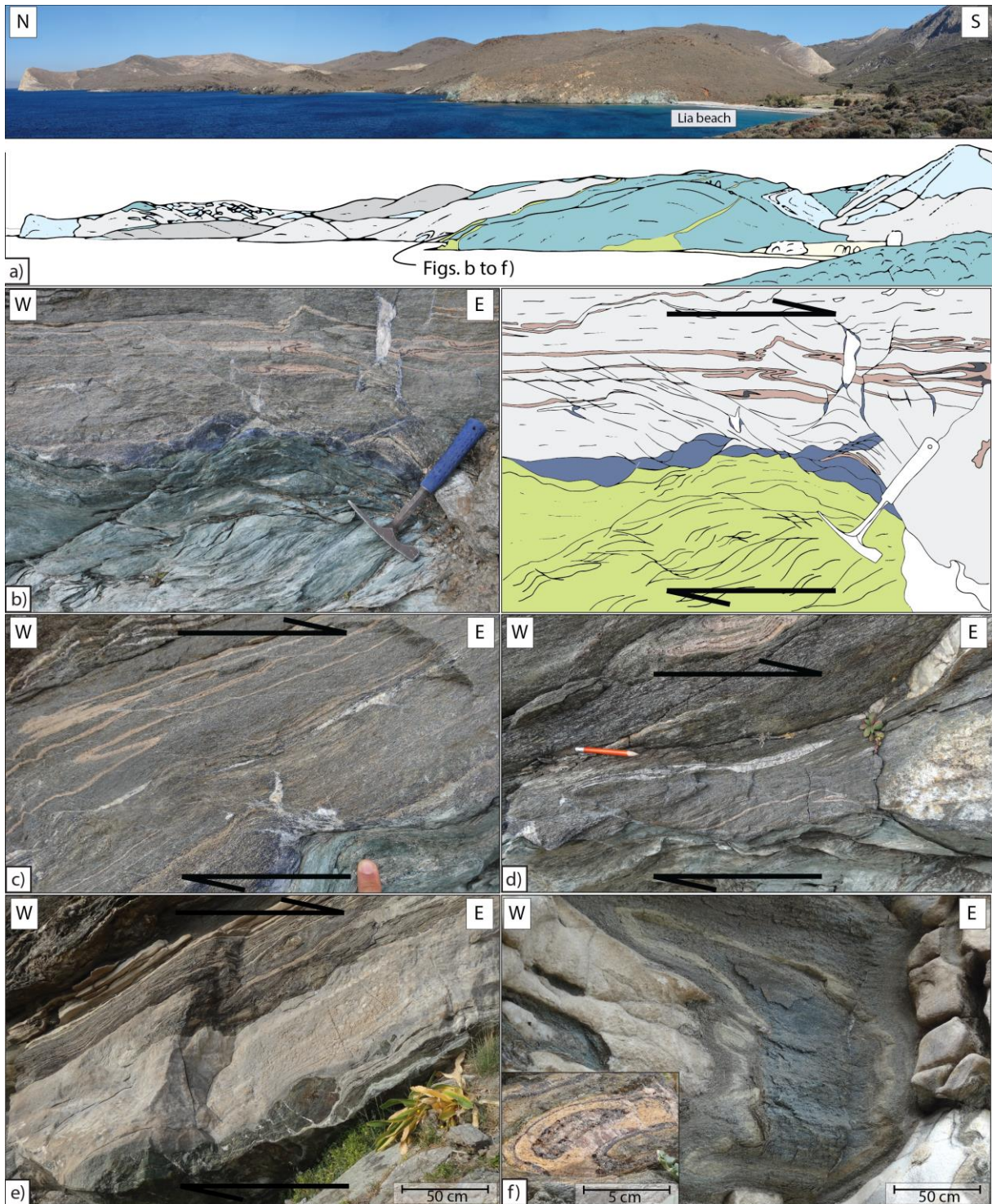
491 that preserved eclogite- to blueschist-facies parageneses, rocks of the Chroussa Subunit are
 492 strongly overprinted in greenschist-facies conditions all along the contact (Figs. 11c, 11d).
 493



494
 495 Figure 11: Basal contact of the Kampos metabasite belt: the Kastri Shear Zone. Pictures are located on the Fig.
 496 12. a) Field view and its interpretation of the eastern part of the Kastri Shear Zone. Large-scale asymmetric
 497 boudins of marble are observed in the contact zone and show top-to-the northeast sense of deformation. b) Zoom
 498 showing the intense folding of black marbles below this contact. c) Directly below the contact, the Chroussa
 499 Subunit is highly retrogressed and displays syn-greenschist top-to-the east sense of shear. d) High-pressure
 500 glaucophanites bearing lawsonite pseudomorphs are well preserved up to the contact on Lia Beach.
 501

502 Although the Kampos Subunit composes the upper structural part of the CBU, a klippe
503 with a lithology similar to Chroussa Subunit is observed above the Kampos metabasite belt
504 (Fig. 10). The contact zone between this klippe and the roof of the Kampos metabasite belt
505 displays intense deformation and occurs between foliated serpentinite and metapelite (Figs.
506 12a, 12b). The foliation is parallel to the contact and is cut by a significant number of east-
507 dipping shear zones decorated with syn-kinematic glaucophanes (Figs. 12b, 12c, 12d). This
508 shear zone also shows asymmetrical boudins of metabasites included in a sigmoidal foliation
509 compatible with top-to-the east shearing deformation and folds with curved axes mostly
510 parallel to the stretching lineation, suggesting sheath folds (Figs. 12e, 12f). All these
511 structures define the existence of a major syn-blueschist top-to-the east shear zone located at
512 the roof of the Kampos metabasite belt, which we called the Lia Shear Zone.

513



514
 515 Figure 12: Roof contact of the Kampos metabasite belt. a) Field view of the western part of the Kampos
 516 metabasite belt and its geological interpretation. b, c, d) This contact is characterized by serpentinites below and
 517 metapelites on top, both affected by top-to-the east syn-blueschist shear bands. e) Asymmetric boudinage of a
 518 metabasite layer included in a sigmoidal foliation compatible with top-to-the east shearing deformation. f) Folds
 519 with curved axes sub-parallel to the stretching lineation and showing closed contour building the typical eye-
 520 structure of sheath folds.

521

522

523 5.3) CBU-Vari Unit contact: the Vari Detachment

524

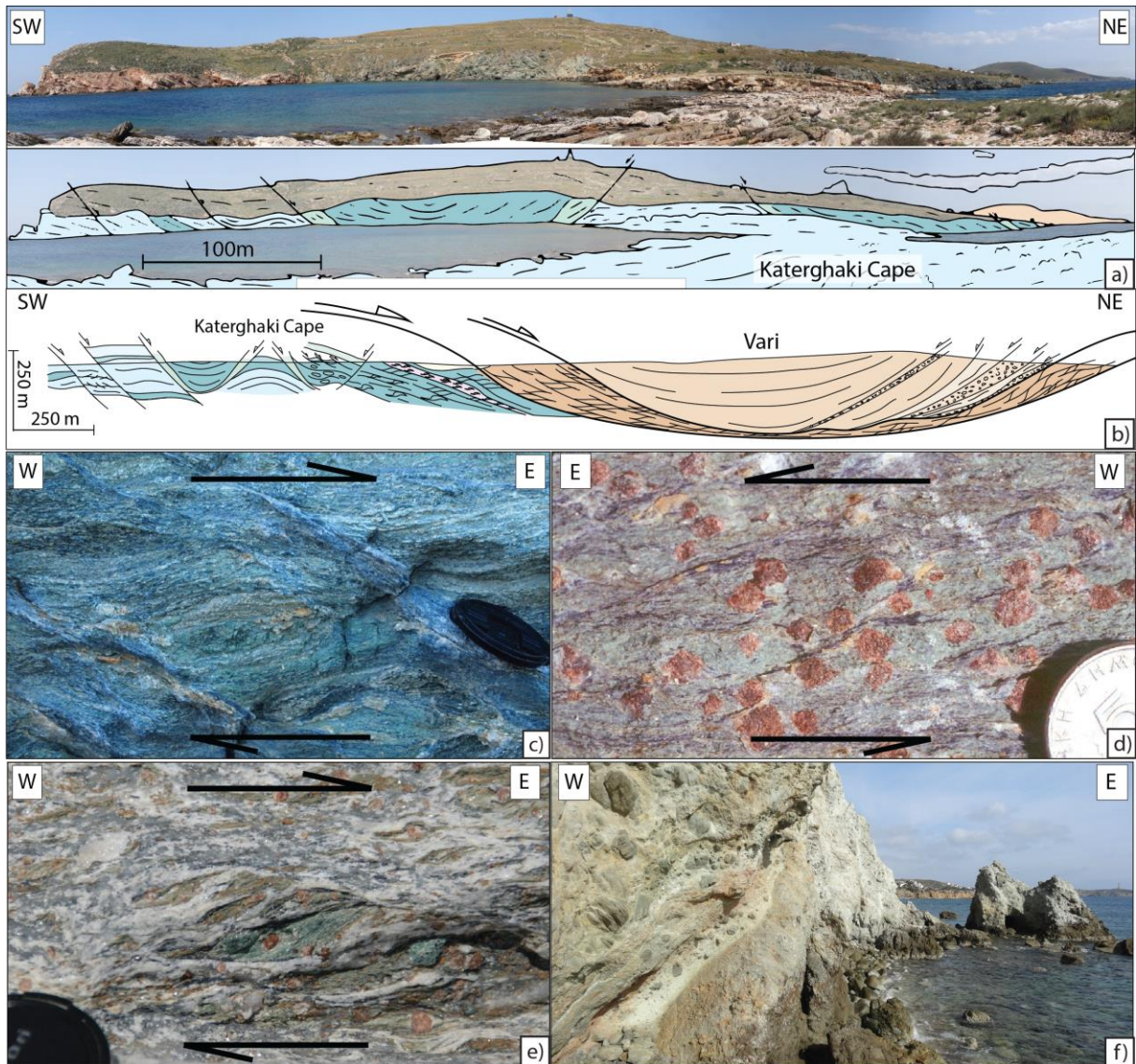
525 The contact between the CBU and Vari Unit is a debated topic in literature. The contact
526 itself is hidden by Quaternary deposits and probably affected by late normal faults. However,
527 field investigations into the footwall unit, i.e. the CBU, allow proposing new arguments on
528 the internal architecture of the Vari Detachment from bottom to top as it crops out from Cape
529 Katerghaki to Vari (Fig. 13).

530 Below the contact, trending parallel to the stretching lineation, the whole section is
531 characterized by a shallow northeast-dipping foliation showing that Vari Unit structurally
532 overlain Kampos Subunit (Figs. 13a, 13b). As the rest of Kampos Subunit, these mafic rocks
533 preserve HP-LT metamorphic parageneses such as eclogites and blueschists (see also [Trotet et](#)
534 [al., 2001a](#)), and display a gradient of retrogression from eclogite- to blueschist-facies toward
535 the contact. Indeed, the southwestern part of Cape Katerghaki (see location on Fig. 3) is
536 composed of 10 m-thick massive eclogite bodies, which are more and more retrogressed in
537 the blueschist-facies toward Vari Unit. All along this gradient, rocks show evidence of syn-
538 eclogitic stretching reworked by syn-blueschists top-to-the east ductile shearing with HP-LT
539 minerals such as glaucophanes decorating shear zones (Figs. 13c, 13d). South of Fabrika
540 beach, structurally 20-30 m below the contact, a metaconglomerate composed of eclogitized
541 mafic pebbles comprised within a marble matrix show top-to-the east sense of shear (Fig. 13e).
542 Conjugate northeast-striking normal faults displace the inherited high-pressure structure by a
543 few tens of meters. This may be due to conjugate normal faults (Figs. 13a, 13b).

544 Just above the contact and within the Vari Unit, mylonitic greenschists are observed,
545 displaying only greenschist-facies metamorphism without any evidence of prior HP-LT stage,
546 in contrast with the greenschist-facies metamorphic rocks observed in the bulk of the CBU.
547 These rocks are strongly foliated and top-to-the E/NE shear criteria are observed such as

548 sigmoidal pressure shadows on pyrite showing top-to-the east kinematic in the north of
549 Fabrika beach, and top-to-the northeast shear bands south of Azolimnos village. On top of
550 these greenschist-facies mylonites, the Vari orthogneiss shows a plano-linear ductile fabric
551 with a stretching lineation oriented N70°E, intercalated in some places with fine-grained
552 amphibolites. This unit is affected by brittle deformation, expressed as several 10 m-thick
553 zones of cataclasites cutting through the orthogneiss (Fig. 13f; see also [Soukis and Stöckli,](#)
554 [2013](#)). Several E-W trending normal faults are observed in this area, cutting across the
555 orthogneiss foliation at distance from the contact with the CBU, at variance with Philippon et
556 al.'s ([2011](#)) interpretation of the regional structure. Our interpretation is confirmed at larger
557 scale. Philippon et al. (2011) correlated the Vari basement lithologies with the so-called
558 gneiss observed in the lower part of our Posidonia Unit, but we have seen that Posidonia Unit
559 has seen the same peak of metamorphism as the other CBU of Syros with the local
560 preservation of blueschists- or eclogite-facies metabasites while the Vari Unit has never been
561 through HP-LT conditions.

562



563
 564 Figure 13: The Vari Detachment. a) Field photography showing that the CBU is structurally below the Vari Unit.
 565 b) Cross-section showing the architecture of the Vari Detachment and its top-to-the east sense of motion. c, d, e)
 566 Below the Vari Detachment, rocks of the CBU display a significant number of top-to-the east syn-blueschist
 567 shear bands affecting eclogites. f) Large-scale cataclastic zones observed upon the Vari Detachment within the
 568 gneiss of Vari.

569
 570

571 6) Discussion

572

573 Although our new geological map matches the one of Keiter et al. (2011) from a
 574 lithological point of view, its structural interpretation is drastically different. This is
 575 particularly evident in the analysis of large-scale geometries, unit and subunit subdivisions

576 and in the analysis of metamorphic record, which allowed us to identify several orders of
577 shear zones due to strain localization.

578

579 6.1) What is left of the original nappe structure of the Cycladic Blueschist Unit?

580

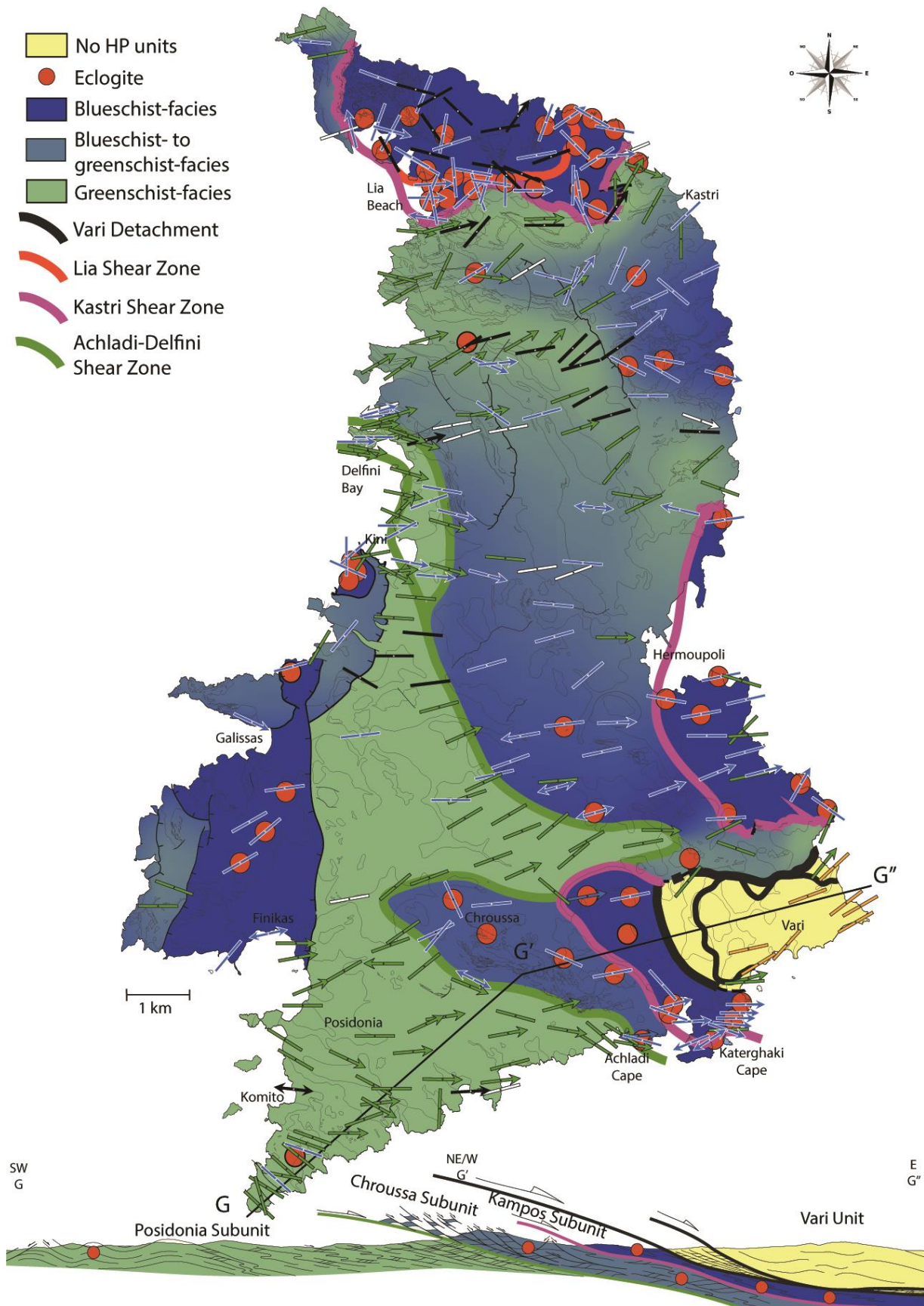
581 We have recognized three distinct tectonic subunits composing the CBU in Syros,
582 from top to base, the Kampos, Chroussa and Posidonia subunits, all resting structurally below
583 the Vari Unit, which shows no evidence of HP. These subunits are characterized by their
584 lithology and predominant metamorphic facies as seen in the field. All three subunits have
585 seen the P-T conditions of the eclogite-facies but they have been subjected to different
586 degrees of retrogression during exhumation. Following our observations, we propose a new
587 metamorphic map based upon the study of predominant metamorphic facies, as well as on
588 kinematic indicators and their relation to metamorphic parageneses (Fig. 14). This map, where
589 colors correspond to the predominant metamorphic facies, displays the first-order distribution
590 of the main parageneses.

591 The recognition of remains of eclogite within all three subunits implies that Kampos,
592 Chroussa and Posidonia subunits have all undergone a HP-LT metamorphic event in the
593 eclogite-facies. It ensues that local blueschist- or greenschist-facies rocks abundance is
594 retrograde. The degree of retrogression, whether it occurred under blueschist and/or
595 greenschist metamorphic conditions, is entirely different. Retrogression increases from top to
596 bottom of the CBU, which points to important differences in the P-T-time evolution of the
597 different subunits during exhumation, as previously proposed by Trotet et al. (2001b). The
598 imprint of deformation during exhumation has been different in each of these subunits,
599 intense in the lowermost Posidonia Subunit (where the entire subunit has been sheared and
600 pervasively retrogressed), weaker in the uppermost Kampos Subunit (where blueschist- and

601 then greenschist-facies deformation is localized along preferential shear zones). The Achladi-
602 Delfini Shear Zone best shows this contrast. These features are similar to those observed on
603 Sifnos (Roche et al., submitted) and seem characteristic of the large-scale structure acquired
604 by the CBU within the subduction channel before those rocks were reworked by greenschist-
605 facies deformation during Oligocene to Miocene extension. We now discuss the
606 tectonometamorphic evolution of the subunits within the subduction channel.

607 The apparent inverse metamorphic gradient defined by the transition from the
608 preserved high-pressure Kampos Subunit to the strongly retrograded Posidonia Subunit raises
609 petrological questions. Indeed, very different P-T histories were so far published for Syros in
610 terms of peak P-T conditions and shape of retrograde P-T path (Fig. 1b). Exhumation
611 scenarios with a single retrograde P-T path for the whole CBU (Keiter et al., 2004, 2011;
612 Schumacher et al., 2008) cannot explain the different degrees of retrogression observed in the
613 CBU. Maximum P-T conditions around 15kbar and 500°C (Schumacher et al., 2008) just
614 fringe the eclogite-facies (Fig. 1b) while eclogites are abundantly observed on Syros as well
615 as on Sifnos (Trotet et al., 2001a). To justify these apparent contradictions, Schumacher et al.
616 (2008) hypothesized that eclogites of Syros are the product of an earlier metamorphic event
617 and were juxtaposed with the rest of the CBU by tectonic contacts. As result of our
618 observations, the presence of eclogite boudins and lenses in all subunits cropping out on Syros,
619 except the Vari Unit, does not fit the interpretation of Schumacher et al. (2008). An
620 alternative explanation would be that the glaucophane-bearing marbles studied by
621 Schumacher et al. (2008) were formed during the retrograde path in P-T conditions for which
622 this assemblage is in equilibrium or that the amphibole mineralogy and stability is chemically
623 buffered by the lithology. Indeed, much of the blueschist-facies parageneses on Syros are syn-
624 kinematic and show top-to-the east sense of shear and clearly postdates the eclogite-facies.
625 Consequently, our structural observations best fit the petrological analyses of Trotet et al.

626 (2001b), for whom all subunits of the CBU attained the same metamorphic peak in the P-T
627 field of eclogite-facies, and followed different retrograde P-T paths, leading to different grade
628 of retrogression in the CBU during the continuous activity of large-scale top-to-the east shear
629 zones between Kampos, Chroussa and Posidonia subunits all over the exhumation (Fig. 1b).
630 According to this interpretation, the tectonic history and the metamorphic path to the surface
631 differ from the one envisaged by Keiter et al. (2004, 2011), who suggested rigid block
632 exhumation mechanisms of the whole CBU as a single block. It remains true however that
633 deformation progressively localized during exhumation along shear zones and that entire parts
634 of the islands escape from the low-temperature deformation, these domains are those where
635 the HP-LT parageneses are best preserved, as discussed in the next section.



636
637
638
639
640

Figure 14: New metamorphic map of Syros showing an apparent inverse metamorphic gradient. The G-G'' cross-sections represent a synthetic view over the overall tectonometamorphic structure of Syros. The architecture of the CBU is subdivided here in three subunits separated by large-scale shear zones. Note that in our interpretation, the Vari Detachment juxtaposed with a top-to-the east motion the CBU and the uppermost Vari Unit.

641 6.2) Prograde or retrograde deformation?

642

643 A number of previous structural studies reported that prograde deformation is
644 observed in Syros (Rosenbaum et al., 2002; Keiter et al., 2004, 2011; Philippon et al., 2011).
645 Some of these studies postulated that this deformation took place just before or during peak
646 metamorphism with no or only local retrograde deformation (Rosenbaum et al., 2002; Keiter
647 et al., 2004, 2011). Three main arguments are presented in the literature. 1) The observation
648 of deformed pseudomorphs of lawsonite: Philippon et al. (2011) noted that these
649 pseudomorphs are always sheared with top-to-the S/SW kinematics and they correlated this
650 sense of shear with subduction-related prograde thrusting. 2) The presence of large thrust
651 zones, often described at the base of metabasic units. 3) The widespread preservation of
652 aragonite pseudomorphs supports the view that no pervasive retrograde deformation occurred
653 subsequently to the main prograde to peak metamorphism deformation event. The frequent
654 presence of aragonite pseudomorphs in the Kampos Subunit, for instance in
655 metaconglomerates, indeed shows that no significant deformation occurred at those places in
656 the greenschist-facies and that parts of this subunit were exhumed as rigid bodies once they
657 had exited blueschist-facies conditions (Schumacher et al., 2008).

658 Our study shows that the three subunits composing the CBU are each separated by
659 top-to-the E/NE shear zones (Figs. 3, 14). This top-to-the E/NE deformation event observed
660 within the entire volume of the CBU on Syros also affects lawsonite pseudomorphs (Fig. 6b)
661 in contradiction with Philippon et al.'s observations (2011). Therefore, these structures are not
662 only markers of prograde deformation, but also characterize early retrograde deformation.
663 Indeed, taking into account the new lawsonite + glaucophane out reaction calculated for Fe-
664 Mg end-member at $X_{CO_2} = 0,01$ (Schumacher et al., 2008), and the P-T path of Trotet et al.

665 (2001b), it appears that lawsonite could have been sheared with top-to-the east sense of shear
666 during the first exhumation stages (Fig. 1b).

667 Geometry of the basal contact of the Kampos metabasite belt is quite complex and
668 interpreted differently in previous studies. On one hand, Trotet et al. (2001a) describe this
669 contact as a ductile detachment. For these authors, this contact is marked in the field by an
670 apparent metamorphic gap between retrograded greenschist-facies rocks below the
671 detachment and preserved eclogite- and blueschist-facies above (Fig. 2a). On the other hand,
672 Keiter et al. (2004, 2011) and Philippon et al. (2011) described this contact as a large prograde
673 thrust related to the subduction phase. Although Keiter et al. (2004) challenged the existence
674 of a sharp metamorphic transition through this contact, we confirm this observation of Trotet
675 et al. (2001a). Indeed, the contact zone is clearly marked by retrogression of the upper part of
676 the underlying Chroussa Subunit over a 100 m-thick greenschist-facies shear zone. Moreover,
677 all shear criteria observed within this shear zone are top-to-the E/NE, in agreement with syn-
678 greenschist retrograde sense of shear observed within the Achladi-Delfini Shear Zone deeper
679 down in the CBU. This does not preclude the possibility that the Kampos-Chroussa subunits
680 contact is originally a thrust as it superimposes the Kampos Subunit, which is mostly
681 ophiolitic, on top of the Chroussa Subunit, which is mostly made of metasediments. Our
682 interpretation is that this thrust has been later reactivated as a major top-to-the east shear zone
683 during exhumation. In the same way, we interpret the klippe of Chroussa Subunit, which is
684 structurally positioned above the Kampos metabasite belt (Fig. 10), as thrusting onto the
685 Kampos Subunit during the late prograde phase of subduction or during the early phase of
686 exhumation. Indeed, this klippe corresponds lithologically to the Chroussa Subunit but shows
687 only eclogite to blueschist parageneses as the Kampos Subunit (Fig. 14). Our observations
688 show that this thrust was reactivated only in the blueschist-facies forming the Lia Shear Zone

689 (Fig. 12). Then the klippe and the Kampos metabasite belt may have followed, as a single unit,
690 the same exhumation history.

691 In agreement with Trotet et al. (2001a), one of the major results of our study is the
692 observation of a pervasive continuum of top-to-the E/NE deformation from P-T conditions of
693 the metamorphic peak (eclogite-facies) to late stages of retrogression in the blueschist- and
694 then greenschist-facies. In contrast to Rosenbaum et al. (2002), and Keiter et al. (2004, 2011),
695 we conclude that a large part of the deformation in Syros was acquired during exhumation and
696 that this deformation was heterogeneously distributed and preferentially localized along
697 extensional shear zones.

698 However, it is also clear that locally, criteria of prograde or peak-metamorphism
699 deformations are preserved. Different structures are most notably inconsistent with a
700 pervasive top-to-the E/NE retrograde shearing. First, the orientation of stretching lineations is
701 distinctly scattered in subunits best preserving eclogite and blueschist-facies parageneses (i.e.
702 Chroussa and Kampos subunits; Figs. 3, 4). Indeed, a group of N-S oriented lineations and
703 top-to-the S/SW kinematic indicators, already observed by Philippon et al. (2011), can be
704 found in Kampos Subunit. Then, at a larger-scale, the N-S orientation of the Kampos
705 metabasite belt (see Keiter et al., 2004, 2011) is inconsistent with E-W oriented deformation
706 and top-to-the E/NE sense of shear. All these structures appear to be related with a N-S
707 oriented shearing event and not with the retrograde top-to-the E/NE continuum of
708 deformation described in this study. A plausible explanation would be that these structures
709 were acquired during an early N-S oriented prograde event in the subduction channel, leading
710 to formation of large thrust planes between units that are now found preserved in the highly
711 metamorphic Kampos and Chroussa subunits. This interpretation is consistent with top-to-the
712 S/SW prograde sense of shear described by Philippon et al. (2011). Such peak-metamorphic
713 structures were later reactivated as weak contact zones during exhumation, within a top-to-the

714 E/NE non-coaxial regime progressively localizing strain toward the lower structural parts of
715 the CBU. These features are discussed in the context of the heterogeneous localization of
716 deformation during exhumation of the CBU.

717

718 6.3) Localization of deformation during exhumation

719

720 The roof contact of the Kampos metabasite belt is only marked by syn-blueschist
721 deformation, showing that this shear zone was deactivated early in the exhumation process,
722 and that the deformation localized progressively in the basal contact of Kampos Subunit,
723 which is characterized by syn-greenschist deformation. In contrast with Posidonia Subunit,
724 Chroussa Subunit is not totally retrogressed in the greenschist-facies and shows large portions
725 characterized by the predominance of blueschist-facies parageneses. Once again, this feature
726 illustrates the progressive localization of deformation during exhumation toward the base of
727 the CBU, i.e. toward Posidonia Subunit. Finally, the Achladi-Delfini Shear Zone is currently
728 characterized by syn-greenschist deformation that has overprinted the entire volume of
729 Posidonia Subunit.

730 Progressive localization of deformation toward the base of the CBU in Syros during
731 exhumation is linked with a younging of apparent ages towards the south, from Kampos (45-
732 50 Ma, syn-orogenic period) to Posidonia subunits (20-35 Ma, post-orogenic period),
733 especially shown by $^{40}\text{Ar}/^{39}\text{Ar}$ and Rb/Sr data on white micas (Fig. 2b; [Maluski et al., 1987](#);
734 [Tomaschek, et al., 2003](#); [Putlitz, et al., 2005](#); [Huet, 2010](#); [Bröcker et al., 2013](#)). A possible
735 explanation would be that structurally downward strain localization leads to partial resetting
736 of isotopic systems or even recrystallization in the lowermost units. This migration of
737 deformation could be enhanced by different factors such as intense fluid circulations in the
738 basal part of the CBU and/or increased thermal influx at the base of the metamorphic pile

739 ([Matthews and Schliestedt, 1984](#); [Schliestedt and Matthews, 1987](#); [Avigad, 1993](#); [Trotet et al.,](#)
740 [2001b](#)). This localization could be also linked to the different lithologies composing the CBU
741 on Syros, less and less resistant to deformation toward the base, passing from massive
742 metabasite in Kampos Subunit to a succession of thick marble layers and metapelites in
743 Chroussa Subunit and finally metapelites in Posidonia Subunit. During cooling of
744 metamorphic units, this inherited rheological heterogeneity may have enhanced the downward
745 localization of deformation toward the weak rheological units. So, while Posidonia Subunit
746 has been deformed until the P-T conditions of the greenschist-facies, the Kampos Subunit and
747 parts of the Chroussa Subunit have been only deformed during the first steps of exhumation.
748 This participated to the local preservation of prograde markers of deformation seen today,
749 allowing detailed petrological and structural information to be retrieved on the prograde
750 subduction-related phase of deformation.

751

752 6.4) Thrusting, exhumation and extension

753

754 The contacts between Kampos, Chroussa and Posidonia subunits have a polyphase
755 history. The first stage corresponds to the stacking of units by thrusting (i.e. nappe stacking),
756 probably during the prograde evolution and at the pressure peak. A limited number of
757 outcrops suggest that the sense of shear was toward the south during this first episode
758 ([Philippon et al., 2011](#)). The main evidence of thrusting is that the uppermost HP-LT Kampos
759 Subunit is mostly made of ophiolitic material, while the lowermost Posidonia Subunit is rich
760 in metapelites that may have been deposited over a continental basement ([Keiter et al., 2004](#);
761 [2011](#); [Schumacher et al., 2008](#); [Philippon et al., 2011](#)). In a second stage, the contacts were
762 reactivated during the retrograde evolution and exhumation, via a top-to-the east shearing
763 deformation, localized along the main contacts or distributed within the whole Posidonia

764 Subunit. This continuum of top-to-the east shear thus encompasses two major periods of the
765 geodynamic evolution of the Aegean: (1) The Eocene construction of the Hellenides nappe
766 stack and HP-LT accretionary complex of the CBU; (2) the Oligocene to Miocene extension
767 leading to crustal thinning and formation of the Aegean Sea in the back-arc region of the
768 Hellenic subduction. The first period corresponds to exhumation of the CBU within the
769 subduction channel (syn-orogenic exhumation, [Jolivet et al., 2003](#); [Jolivet and Brun, 2010](#)),
770 and the second stage to the formation of metamorphic core complexes of the Cyclades (post-
771 orogenic extension, [Huet et al., 2011](#)).

772

773 6.5) The Vari Detachment: an example of a subduction channel roof

774

775 Several studies describe the existence of the Vari Detachment on Syros, juxtaposing
776 the Vari Unit above the CBU ([Trotet et al., 2001a](#); [Rosenbaum et al., 2002](#); [Ring et al., 2003](#);
777 [Jolivet et al., 2010](#); [Keiter et al., 2011](#); [Soukis and Stöckli, 2013](#)). It is also suggested that this
778 detachment reappears on the neighboring island of Tinos ([Maluski et al., 1987](#); [Patzak et al.,](#)
779 [1994](#); [Jolivet et al., 2010](#); [Soukis and Stöckli, 2013](#)). This assumption is based on similar
780 structural and metamorphic features of the footwall and hangingwall of the detachment
781 outcropping in each island. On the other hand, [Philippon et al. \(2011\)](#) drastically revised the
782 interpretation of this contact, repositioning the Vari Unit below the CBU. According to them,
783 these rocks have to be correlated with the Cycladic Continental Basement cropping out in the
784 southern part of the Cyclades (cf. [Huet et al., 2009](#); [Augier et al., 2015](#)). On the contrary, we
785 demonstrated here, that clear field evidences support the original interpretation putting the
786 Vari Unit on top of the CBU (Figs. 13a, 13b). The Vari Detachment is generally considered as
787 responsible for the exhumation of the CBU ([Trotet et al., 2001a](#); [Jolivet et al., 2010](#); [Soukis](#)
788 [and Stöckli, 2013](#)). [Trotet et al. \(2001a, 2001b\)](#) and [Jolivet et al. \(2010\)](#) argued that the Vari

789 Detachment has accommodated part of the exhumation since the syn-orogenic period,
790 whereas Ring et al. (2003) conclude that this structure only allowed the final exhumation of
791 the CBU. Ring et al. (2003) obtained different retrograde cooling paths at the footwall and at
792 the roof of the Vari Detachment with fission-tracks data on apatite and zircon gathered on
793 Syros (Fig. 2b) and Tinos. From their results, they derive that intra-arc distributed extension
794 caused only the final 6-9 km of vertical exhumation, and they conclude that the Vari
795 Detachment was characterized by fast extension but caused little exhumation. But this
796 detailed study is based upon fission-track data, which put only T-t constraints on the final
797 parts of exhumation. Our structural observations show that the top-to-the E/NE deformation
798 affecting the rocks located at the footwall of the Vari Detachment started in eclogite to
799 blueschist P-T conditions and evolved progressively toward the conditions of the greenschist-
800 facies. Cataclastic deformation observed in the Vari Detachment testifies that this detachment
801 has continued to operate in brittle conditions, but not that this detachment started in brittle
802 conditions as asserted by Ring et al. (2003). Huet et al. (2009) and Jolivet et al. (2010)
803 hypothesized that the Vari Detachment represents the Eocene roof of the subduction channel.
804 Then, with the Oligocene to Miocene southward slab retreat, the Vari Detachment was
805 transferred in a back-arc position in the Late Miocene as attested by its present position.

806

807 6.6) Tectonometamorphic evolution of a subduction channel

808

809 Integrating the above presented and discussed new observations with the one available
810 in literature, we propose a new tectonometamorphic evolution sequence. This scenario is
811 divided in four steps:

812 1) From the early Paleocene (65 Ma) to the early Eocene (50 Ma):

813 From the end of the Cretaceous, the Apulian continental block subducted below the southern
814 margin of Eurasia (Jolivet and Brun, 2010). During this N-S oriented subduction phase, the
815 Hellenic nappe stack was progressively constructed. The Pindos oceanic domain probably
816 started to subduct around 55 Ma (Menant et al., 2015) forming at depth the CBU (Bonneau
817 and Kienast, 1982; Jolivet and Brun, 2010). Between 55 and 50 Ma, CBU rocks were strongly
818 deformed, forming the observed N-S trending stretching lineation, resulting in the thrusting of
819 subunits such as the Kampos Subunit with a resultant top-to-the S/SW sense of shear
820 associated with prograde shear zones (Philippon et al., 2011) and large-scale open folds
821 (Keiter et al., 2011; see also Roche et al., submitted, for Sifnos Island).

822 2) From the early Eocene (50 Ma) to the early Oligocene (35-30 Ma):

823 The CBU started to exhume, following an initial cold retrograde P-T path able to preserve
824 HP-LT parageneses. Ductile shear zones associated with syn-blueschist top-to-the east sense
825 of shear accommodated this exhumation below the Vari Detachment that represented the roof
826 of the subduction channel. During this syn-orogenic phase, deformation started to localize at
827 the interface between large lithological units, probably along former thrusts, delimiting the
828 subunits detached from the overlying plate. During this period, a top-to-the south thrust,
829 observed on Ios Island and located at the base of the CBU (Huet et al., 2009), was active and
830 exhumation of the CBU was accommodated within the subduction channel of a slowly
831 retreating subduction zone while the thrust front was propagated southward (Jolivet et al.,
832 2003; Brun and Faccenna, 2008; Jolivet and Brun, 2010; Ring et al., 2010).

833 3) From the early Oligocene (30-35 Ma) to the early Miocene (23-19 Ma):

834 A drastic change in kinematic boundary conditions occurs at 30-35 Ma with a decrease of the
835 absolute northward motion of Africa and the southward retreat of the subducting slab (Jolivet
836 and Faccenna, 2000). This drastic change marks the transition from syn-orogenic exhumation
837 to post-orogenic extension and the formation of the Aegean Sea. The post-orogenic

838 extensional regime is still characterized by top-to-the E/NE sense of shear as observed in the
839 Achladi-Delfini Shear Zone. During exhumation, deformation progressively localized in
840 lower structural levels of the CBU where retrogression is almost complete.

841 4) From the Early Miocene (23-19 Ma) to the present:

842 The final exhumation of the CBU is first controlled by ductile-brittle normal faults and finally
843 by purely brittle normal faults. The Achladi-Delfini Shear Zone displays ductile-brittle
844 deformation with top-to-the E/NE sense of shear, like some outcrops in the Chroussa Subunit.
845 Large-scale brittle normal faults can finally affect the exhumed units such as the 4 km
846 Finikas-Galissas Fault, which juxtaposes well-preserved eclogite- to blueschist-facies rocks
847 with strongly retrogressed units (Figs. 3, 8b).

848

849 7) Conclusion

850

851 In this study, new geological and metamorphic maps and cross-sections of Syros have
852 been proposed, described and discussed. Field mapping combined with structural and
853 petrological observations allow us to subdivide the CBU into three subunits, Kampos,
854 Chroussa and Posidonia subunits, separated by major ductile shear zones. Eclogite is found
855 within all three subunits. This implies that, despite their entirely different degree of
856 retrogression (from eclogite at the top to greenschist at the base), the subunits have undergone
857 the same HP-LT metamorphic peak in eclogite-facies, pointing to important differences in P-
858 T-time evolution during exhumation. Large-scale ductile shear zones delimiting the subunits
859 record a multi-stage structural evolution. They may have formed during burial with the
860 development of a currently N-S trending eclogite to blueschist stretching lineation
861 accompanied by top-to-the S/SW sense of shear. From the P-T conditions of the metamorphic
862 peak and during exhumation, the contacts were reactivated as top-to-the east ductile

863 extensional shear zones. New observations of the Vari Detachment, which juxtaposes the low-
864 pressure Vari Unit onto the CBU, show consistent top-to-the-east shear sense. We infer that,
865 after the prograde top-to-the S/SW deformation, the CBU was exhumed by an overall top-to-
866 the east shearing all the way from the depth of the eclogite-facies to the greenschist-facies and
867 finally, into the brittle crust. During exhumation, deformation progressively localized
868 downward in the CBU, along several large-scale ductile shear zones, allowing preservation of
869 earlier HP-LT structures and metamorphic parageneses.

870 This study brings new insights on the tectonometamorphic evolution of a subduction
871 channel, showing progressive strain localization, during both the prograde and retrograde
872 history. The rate of this progressive strain localization is however unknown, and in general,
873 poorly known in similar geological contexts. Are all shear zones coeval, do they work at the
874 same time or can we see a sequential development until final localization on the brittle Vari
875 Detachment? As an open question left for further work, we can say that modeling the
876 evolution of the CBU accretionary complex and understanding the mechanical behavior of the
877 subduction interface requires quantifying the rate of strain localization. Acquisition of
878 detailed time constraints along the P-T path is fundamental in determining the role and the
879 importance of the shear zones bounding the subunits of Syros, it is a pre-requisite for further
880 considerations on exhumation mechanisms.

881

882 Acknowledgments

883 This work has received funding from the European Research Council (ERC) under the
884 seventh Framework Programme of the European Union (ERC Advanced Grant, grant
885 agreement No 290864, RHEOLITH) and from the Institut Universitaire de France. It is a
886 contribution of the Labex VOLTAIRE. We forward our warmest thanks to Catherine and
887 Jacques Arvanitis for their magnificent hospitality and friendship all through the years since

888 1994 when L. Jolivet stayed at Alkyon Hotel just by chance for the first time. The authors are
889 grateful to S. Janiec and J.G. Badin (ISTO) for the preparation of thin sections. We thank A.
890 Beaudoin and M. Ducoux for pertinent remarks and Bernhard Grasemann and an anonymous
891 reviewer for insightful suggestions.

892

893 References

894

- 895 Altherr, R., Kreuzer, H., Wendt, I., Lenz, H., Wagner, G.A., Keller, J., Harre, W., Hohndorf, A., 1982. A late
896 Oligocene/early Miocene high temperature belt in the Attic-Cycladic crystalline complex (SE
897 Pelagonian, Greece). *Geologisches Jahrbuch E* 23, 97–164.
- 898 Altherr, R., Schliestedt, M., Okrusch, M., Seidel, E., Kreuzer, H., Harre, W., Lenz, H., Wendt, I., Wagner, G.A.,
899 1979. Geochronology of high-pressure rocks on Sifnos (Cyclades, Greece). *Contributions to*
900 *Mineralogy and Petrology* 70, 245–255.
- 901 Altherr, R., Siebel, W., 2002. I-type plutonism in a continental back-arc setting: Miocene granitoids and
902 monzonites from the central Aegean Sea, Greece. *Contrib Mineral Petrol* 143, 397–415.
903 doi:10.1007/s00410-002-0352-y
- 904 Andersen, T.B., Osmundsen, P.T., Jolivet, L., 1994. Deep crustal fabrics and a model for the extensional
905 collapse of the southwest Norwegian Caledonides. *Journal of Structural Geology* 16, 1191–1203.
- 906 Andriessen, P.A.M., Banga, G., Hebeda, E.H., 1987. Isotopic age study of pre-Alpine rocks in the basal units on
907 Naxos, Sikinos and Ios, Greek Cyclades. *Geologie en Mijnbouw* 66, 3–14.
- 908 Andriessen, P.A.M., Boelrijk, N., Hebeda, E.H., Priem, H.N.A., Verdurnen, E.A., Verschure, R.H., 1979. Dating
909 the events of metamorphism and granitic magmatism in the Alpine Orogen of Naxos (Cyclades,
910 Greece). *Contributions to Mineralogy and Petrology* 69, 215–225.
- 911 Ashley, K.T., Caddick, M.J., Steele-MacInnis, M.J., Bodnar, R.J., Dragovic, B., 2014. Geothermobarometric
912 history of subduction recorded by quartz inclusions in garnet. *Geochemistry, Geophysics, Geosystems*
913 15, 350–360.
- 914 Augier, R., Jolivet, L., Gadenne, L., Lahfid, A., Driussi, O., 2015. Exhumation kinematics of the Cycladic
915 Blueschists unit and back-arc extension, insight from the Southern Cyclades (Sikinos and Folegandros
916 Islands, Greece), *Tectonics*, 34, doi: 10.1002/2014TC003664. Received 24, 2.
- 917 Austrheim, H., Griffin, W. L., 1985. Shear deformation and eclogite formation within granulite-facies
918 anorthosites of the Bergen Arcs, western Norway. *Chemical Geology* 50, 267–281.
- 919 Avigad, D., 1993. Tectonic juxtaposition of blueschists and greenschists in Sifnos Island (Aegean Sea) ;
920 implications for the structure of the Cycladic blueschist belt. *Journal of Structural Geology* 15, 1459–
921 1469.
- 922 Avigad, D., Garfunkel, Z., 1991. Uplift and exhumation of high-pressure metamorphic terrains: the example of
923 the Cycladic blueschist belt (Aegean Sea). *Tectonophysics* 188, 357–372.
- 924 Beaudoin, A., Laurent, V., Augier, R., Rabillard, A., Jolivet, L., Arbaret, L., and Menant, A., 2015, The Ikaria
925 Metamorphic Core Complex between the Cyclades and the Menderes massif: submitted.
- 926 Bell, T.H., Brothers, R.N., 1985. Development of P-T prograde and P-retrograde, T-prograde isogradic surfaces
927 during blueschist to eclogite regional deformation/metamorphism in New Caledonia, as indicated by
928 progressively developed porphyroblast microstructures. *Journal of Metamorphic Geology* 3, 59–78.
- 929 Blake, M.C., Bonneau, M., Geyssant, J., Kienast, J.R., Lepvrier, C., Maluski, H., Papanikolaou, D., 1981. A
930 geological reconnaissance of the Cycladic blueschist belt, Greece. *Geological Society of America*
931 *Bulletin* 92, 247–254.
- 932 Bolhar, R., Ring, U., Allen, C.M., 2010. An integrated zircon geochronological and geochemical investigation
933 into the Miocene plutonic evolution of the Cyclades, Aegean Sea, Greece: Part 1: Geochronology.
934 *Contributions to Mineralogy and Petrology* 160, 719–742.
- 935 Bonneau, M., 1984. Correlation of the Hellenide nappes in the south-east Aegean and their tectonic
936 reconstruction. *Geological Society, London, Special Publications* 17, 517–527.
- 937 Bonneau, M., Blake, M.C., Gueyssant, J., Kienast, J.R., Lepvrier, C., Maluski, H., Papanikolaou, D., 1980a. Sur
938 la signification des séries métamorphiques (schistes bleus) des cyclades (Héllénides, Grèce). *L'exemple*

- 939 de l'île de Syros. CR Seances Acad. Sci. Ser. D 290, 1463–1466.
- 940 Bonneau, M., Kienast, J., Lepvrier, C., Maluski, H., 1980b. Tectonique et métamorphisme haute pression d'âge
941 Eocène dans les Hellénides: exemple de l'île de Syros (Cyclades, Grèce). CR Acad. Sci., Paris 291,
942 171–174.
- 943 Bonneau, M., Kienast, J.R., 1982. Subduction, collision et schistes bleus; l'exemple de l'Egee (Grece). Bulletin
944 de la société Géologique de France 785–791.
- 945 Bröcker, M., Baldwin, S., Arkudas, R., 2013. The geological significance of $^{40}\text{Ar}/^{39}\text{Ar}$ and Rb–Sr white mica
946 ages from Syros and Sifnos, Greece: a record of continuous (re) crystallization during exhumation?
947 Journal of Metamorphic Geology 31, 629–646.
- 948 Bröcker, M., Enders, M., 2001. Unusual bulk-rock compositions in eclogite-facies rocks from Syros and Tinos
949 (Cyclades, Greece): implications for U–Pb zircon geochronology. Chemical Geology 175, 581–603.
- 950 Bröcker, M., Franz, L., 1998. Rb–Sr isotope studies on Tinos Island (Cyclades, Greece): additional time
951 constraints for metamorphism, extent of infiltration-controlled overprinting and deformational activity.
952 Geological Magazine 135, 369–382.
- 953 Bröcker, M., Franz, L., 2006. Dating metamorphism and tectonic juxtaposition on Andros Island (Cyclades,
954 Greece): results of a Rb–Sr study. Geological Magazine 143, 609–620.
- 955 Bröcker, M., Kreuzer, H., Matthews, A., Okrusch, M., 1993. $^{40}\text{Ar}/^{39}\text{Ar}$ and oxygen isotope studies of
956 polymetamorphism from Tinos Island, Cycladic blueschist belt, Greece. Journal of Metamorphic
957 Geology 11, 223–240.
- 958 Bröcker, M., Enders, M., 1999. U–Pb zircon geochronology of unusual eclogite-facies rocks from Syros and
959 Tinos (Cyclades, Greece). Geological Magazine 136, 111–118.
- 960 Brun, J.-P., Faccenna, C., 2008. Exhumation of high-pressure rocks driven by slab rollback. Earth and Planetary
961 Science Letters 272, 1–7.
- 962 Brun, J.-P., Sokoutis, D., 2010. 45 my of Aegean crust and mantle flow driven by trench retreat. Geology 38,
963 815–818.
- 964 Brunet, C., Monié, P., Jolivet, L., & Cadet, J. P., 2000. Migration of compression and extension in the
965 Tyrrhenian Sea, insights from $^{40}\text{Ar}/^{39}\text{Ar}$ ages on micas along a transect from Corsica to Tuscany.
966 Tectonophysics 321, 127–155.
- 967 Buick, I.S., 1991. The late Alpine evolution of an extensional shear zone, Naxos, Greece. Journal of the
968 Geological Society 148, 93–103.
- 969 Burg, J. P., Proust, F., Tapponnier, P., Chen, G. M., 1983. Deformation phases and tectonic evolution of the
970 Lhasa block (southern Tibet, China). Eclogae Geologicae Helvetiae 76, 643–665.
- 971 Denèle, Y., Lecomte, E., Jolivet, L., Lacombe, O., Labrousse, L., Huet, B., Le Pourhiet, L., 2011. Granite
972 intrusion in a metamorphic core complex: the example of the Mykonos laccolith (Cyclades, Greece).
973 Tectonophysics 501, 52–70.
- 974 Dercourt, J., Zonenshain, L.P., Ricou, L.-E., Kazmin, V.G., Le Pichon, X., Knipper, A.L., Grandjacquet, C.,
975 Sbertshikov, I.M., Geysant, J., Lepvrier, C., others, 1986. Geological evolution of the Tethys belt from
976 the Atlantic to the Pamirs since the Lias. Tectonophysics 123, 241–315.
- 977 Dragovic, B., Samanta, L.M., Baxter, E.F., Selverstone, J., 2012. Using garnet to constrain the duration and rate
978 of water-releasing metamorphic reactions during subduction: An example from Sifnos, Greece.
979 Chemical Geology 314, 9–22.
- 980 Duchene, S., Aissa, R., Vanderhaeghe, O., 2006. Pressure-temperature-time evolution of metamorphic rocks
981 from Naxos (Cyclades, Greece): constraints from thermobarometry and Rb/Sr dating. Geodinamica
982 Acta 19, 301–321.
- 983 Dürr, S., Altherr, R., Keller, J., Okrusch, M., Seidel, E., 1978. The median Aegean crystalline belt: stratigraphy,
984 structure, metamorphism, magmatism. Alps, Apennines, Hellenides 38, 455–476.
- 985 Epard, J. L., & Steck, A., 2008. Structural development of the Tso Morari ultra-high pressure nappe of the
986 Ladakh Himalaya. Tectonophysics 451, 242–264.
- 987 Evans, B. W., 1990. Phase relations of epidote-blueschists. Lithos 25, 3–23.
- 988 Faure, M., Bonneau, M., Pons, J., 1991. Ductile deformation and syntectonic granite emplacement during the
989 late Miocene extension of the Aegea (Greece). Bulletin de la Société géologique de France 5, 3–11.
- 990 Gautier, P., 1995. Géométrie crustale et cinématique de l'extension tardiorogénique dans le domaine centre -
991 égéen: Iles des Cyclades et D'eubée (Grèce). Mem. de Geosci. Rennes 61, 417 pp.
- 992 Grasemann, B., Petrakakis, K., 2007. Evolution of the Serifos metamorphic core complex. Inside the Aegean
993 Core Complexes. Journal of the Virtual Explorer, Electronic Edition.
- 994 Grasemann, B., Schneider, D.A., Stöckli, D.F., Iglseder, C., 2012. Miocene bivertent crustal extension in the
995 Aegean: Evidence from the western Cyclades (Greece). Lithosphere L164–1.
- 996 Groppo, C., Forster, M., Lister, G., Compagnoni, R., 2009. Glaucofane schists and associated rocks from
997 Sifnos (Cyclades, Greece): New constraints on the P–T evolution from oxidized systems. Lithos 109,
998 254–273.

- 999 Gupta, S., Bickle, M.J., 2004. Ductile shearing, hydrous fluid channelling and high-pressure metamorphism
1000 along the basement-cover contact on Sikinos, Cyclades, Greece. *Geological Society, London, Special*
1001 *Publications* 224, 161–175.
- 1002 Hausmann, H., 1845. Beiträge zur Oryktographie von Syra. *Journal für Praktische Chemie* 34, 238–241.
- 1003 Hecht, J., 1985. Geological map of Greece 1:50.000, Syros Island: Athens, Institute of Geology and Mineral
1004 Exploration, 1 sheet.
- 1005 Huet, B., 2010. Rhéologie de la lithosphère continentale: L'exemple de la Mer Egée. PhD thesis, Université
1006 Pierre et Marie Curie-Paris VI, 402 pp.
- 1007 Huet, B., Labrousse, L., Jolivet, L., 2009. Thrust or detachment? Exhumation processes in the Aegean: insight
1008 from a field study on Ios (Cyclades, Greece). *Tectonics* 28.
- 1009 Huet, B., Le Pourhiet, L., Labrousse, L., Burov, E., Jolivet, L., 2011. Post-orogenic extension and metamorphic
1010 core complexes in a heterogeneous crust: the role of crustal layering inherited from collision.
1011 Application to the Cyclades (Aegean domain). *Geophysical Journal International* 184, 611–625.
- 1012 Iglseider, C., Grasemann, B., Schneider, D.A., Petrakakis, K., Miller, C., Klötzli, U.S., Thöni, M., Zámolyi, A.,
1013 Rambousek, C., 2009. I and S-type plutonism on Serifos (W-Cyclades, Greece). *Tectonophysics* 473,
1014 69–83.
- 1015 Jansen, J.B.H., 1973. Geological map of Naxos (1/50 000). Nation. Inst. Geol. Mining Res., Athens.
- 1016 Jolivet, L., Brun, J.-P., 2010. Cenozoic geodynamic evolution of the Aegean. *International Journal of Earth*
1017 *Sciences* 99, 109–138.
- 1018 Jolivet, L., Faccenna, C., 2000. Mediterranean extension and the Africa-Eurasia collision. *Tectonics* 19, 1095–
1019 1106.
- 1020 Jolivet, L., Faccenna, C., Goffé, B., Burov, E., Agard, P., 2003. Subduction tectonics and exhumation of high-
1021 pressure metamorphic rocks in the Mediterranean orogens. *American Journal of Science* 303, 353–409.
- 1022 Jolivet, L., Lecomte, E., Huet, B., Denèle, Y., Lacombe, O., Labrousse, L., Le Pourhiet, L., Mehl, C., 2010. The
1023 north cycladic detachment system. *Earth and Planetary Science Letters* 289, 87–104.
- 1024 Jolivet, L., Menant, A., Sternai, P., Rabillard, A., Arbaret, L., Augier, R., Laurent, V., Beaudoin, A., Grasemann,
1025 B., Huet, B., Labrousse, L., Le Pourhiet, L., 2015. The geological signature of a slab tear below the
1026 Aegean. *Tectonophysics*.
- 1027 Jolivet, L., Rimmelé, G., Oberhänsli, R., Goffé, B., Candan, O., 2004. Correlation of syn-orogenic tectonic and
1028 metamorphic events in the Cyclades, the Lycian nappes and the Menderes massif. *Geodynamic*
1029 *implications. Bulletin de la Société Géologique de France* 175, 217–238.
- 1030 Keay, S., 1998. The geological evolution of the Cyclades, Greece: constraints from SHRIMP U-Pb
1031 geochronology. Australian National University.
- 1032 Keay, S., Lister, G., Buick, I., 2001. The timing of partial melting, Barrovian metamorphism and granite
1033 intrusion in the Naxos metamorphic core complex, Cyclades, Aegean Sea, Greece. *Tectonophysics* 342,
1034 275–312.
- 1035 Keiter, M., Ballhaus, C., Tomaschek, F., 2011. A new geological map of the Island of Syros (Aegean Sea,
1036 Greece): Implications for lithostratigraphy and structural history of the Cycladic Blueschist Unit.
1037 *Geological Society of America Special Papers* 481, 1–43.
- 1038 Keiter, M., Piepjohn, K., Ballhaus, C., Lagos, M., Bode, M., 2004. Structural development of high-pressure
1039 metamorphic rocks on Syros island (Cyclades, Greece). *Journal of Structural Geology* 26, 1433–1445.
- 1040 Kuhlemann, J., Frisch, W., Dunkl, I., Kázmér, M., Schmiedl, G., 2004. Miocene siliciclastic deposits of Naxos
1041 Island: Geodynamic and environmental implications for the evolution of the southern Aegean Sea
1042 (Greece). *Geological Society of America Special Papers* 378, 51–65.
- 1043 Labrousse, L., Jolivet, L., Andersen, T.B., Agard, P., Hébert, R., Maluski, H., Schärer, U., 2004. Pressure-
1044 temperature-time deformation history of the exhumation of ultra-high pressure rocks in the Western
1045 Gneiss Region, Norway. *Geological Society of America Special Papers* 380, 155–183.
- 1046 Lagos, M., Scherer, E.E., Tomaschek, F., Münker, C., Keiter, M., Berndt, J., Ballhaus, C., 2007. High precision
1047 Lu-Hf geochronology of Eocene eclogite-facies rocks from Syros, Cyclades, Greece. *Chemical*
1048 *Geology* 243, 16–35.
- 1049 Laurent, V., Beaudoin, A., Jolivet, L., Arbaret, L., Augier, R., and Rabillard, A., 2015. Interactions between
1050 extensional shear zones and syn-tectonic granite intrusion: the example of Ikaria island (Cyclades,
1051 Greece): submitted.
- 1052 Lecomte, E., Jolivet, L., Lacombe, O., Denèle, Y., Labrousse, L., Le Pourhiet, L., 2010. Geometry and
1053 kinematics of a low-angle normal fault on Mykonos island (Cyclades, Greece): Evidence for slip at
1054 shallow dip. *Tectonics* 29.
- 1055 Lee, J., Lister, G.S., 1992. Late Miocene ductile extension and detachment faulting, Mykonos, Greece. *Geology*
1056 20, 121–124.
- 1057 Liou, J. G., Tsujimori, T., Zhang, R. Y., Katayama, I., & Maruyama, S., 2004. Global UHP metamorphism and
1058 continental subduction/collision: the Himalayan model. *International Geology Review* 46, 1–27.

- 1059 Maluski, H., Bonneau, M., Kienast, J.R., 1987. Dating the metamorphic events in the Cycladic area; $^{39}\text{Ar}/^{40}\text{Ar}$
1060 data from metamorphic rocks of the Island of Syros (Greece). *Bulletin de la Société géologique de*
1061 *France* 3, 833–842.
- 1062 Matthews, A., Schliestedt, M., 1984. Evolution of the blueschist and greenschist-facies rocks of Sifnos, Cyclades,
1063 Greece. *Contr. Mineral. and Petrol.* 88, 150–163. doi:10.1007/BF00371419
- 1064 Menant, A., Jolivet, L., Augier, R., Skarpelis, N., 2013. The North Cycladic Detachment System and associated
1065 mineralization, Mykonos, Greece: Insights on the evolution of the Aegean domain. *Tectonics* 32, 433–
1066 452.
- 1067 Menant, A., Jolivet, L., Vrielynck, B., 2015. From crust to mantle dynamics, insight from kinematic
1068 reconstructions and magmatic evolution of the eastern Mediterranean region since the late Cretaceous,
1069 Tectonophysics.
- 1070 Okrusch, M., Bröcker, M., 1990. Eclogites associated with high-grade blueschists in the Cyclades archipelago,
1071 Greece: a review. *European Journal of Mineralogy* 451–478.
- 1072 Parra, T., Vidal, O., Jolivet, L., 2002. Relation between the intensity of deformation and retrogression in
1073 blueschist metapelites of Tinos Island (Greece) evidenced by chlorite–mica local equilibria. *Lithos* 63,
1074 41–66.
- 1075 Patzak, M., Okrusch, M., Kreuzer, H., 1994. The Akrotiri Unit on the island of Tinos, Cyclades, Greece: Witness
1076 to a lost terrane of Late Cretaceous age. (With 18 figures and 8 tables in the text). *Neues Jahrbuch für*
1077 *Geologie und Palaontologie-Abhandlungen* 194, 211–252.
- 1078 Pe-Piper, G., Piper, D.J., Matarangas, D., 2002. Regional implications of geochemistry and style of emplacement
1079 of Miocene I-type diorite and granite, Delos, Cyclades, Greece. *Lithos* 60, 47–66.
- 1080 Peacock, S.M., 1993. The importance of blueschist-eclogite dehydration reactions in subducting oceanic crust.
1081 *Geological Society of America Bulletin* 105, 684–694.
- 1082 Philippon, M., Brun, J.-P., Gueydan, F., 2011. Tectonics of the Syros blueschists (Cyclades, Greece): From
1083 subduction to Aegean extension. *Tectonics* 30.
- 1084 Photiades, A., Keay, S., 2003. Geological and geochronological data for Sikinos and Folegandros metamorphic
1085 units (Cyclades, Greece): Their tectono-stratigraphic significance.
- 1086 Putlitz, B., Cosca, M.A., Schumacher, J.C., 2005. Prograde mica $^{40}\text{Ar}/^{39}\text{Ar}$ growth ages recorded in high
1087 pressure rocks (Syros, Cyclades, Greece). *Chemical Geology* 214, 79–98.
- 1088 Rabillard, A., Arbaret, L., Jolivet, L., Le Breton, N., Gumiaux, C., Augier, R., Grasemann, B., 2015. Interactions
1089 between plutonism and detachments during Metamorphic Core Complex formation, Serifos Island
1090 (Cyclades, Greece). *Tectonics*. DOI: 10.1002/2014TC003650.
- 1091 Raimbourg, H., Jolivet, L., Labrousse, L., Leroy, Y., Avigad, D., 2005. Kinematics of syn-eclogite deformation
1092 in the Bergen Arcs, Norway, implications for exhumation mechanisms. *Special Publication-Geological*
1093 *Society of London* 243, 175–192.
- 1094 Ring, U., Glodny, J., Will, T., Thomson, S., 2010. The Hellenic subduction system: high-pressure metamorphism,
1095 exhumation, normal faulting, and large-scale extension. *Annual Review of Earth and Planetary Sciences*
1096 38, 45–76.
- 1097 Ring, U., Thomson, S.N., Bröcker, M., 2003. Fast extension but little exhumation: the Vari detachment in the
1098 Cyclades, Greece. *Geological Magazine* 140, 245–252.
- 1099 Roche, V., Laurent, V., Cardello, G. L., Jolivet, L., Scaillet, S., submitted. The anatomy of the Cycladic
1100 Blueschist Unit on Sifnos Island (Cyclades, Greece), *Journal of Geodynamics*.
- 1101 Rosenbaum, G., Avigad, D., Sánchez-Gómez, M., 2002. Coaxial flattening at deep levels of orogenic belts:
1102 evidence from blueschists and eclogites on Syros and Sifnos (Cyclades, Greece). *Journal of Structural*
1103 *Geology* 24, 1451–1462.
- 1104 Sanchez-Gomez, M., Avigad, D., Heimann, A., 2002. Geochronology of clasts in allochthonous Miocene
1105 sedimentary sequences on Mykonos and Paros islands: implications for back-arc extension in the
1106 Aegean Sea. *Journal of the Geological Society* 159, 45–60.
- 1107 Schliestedt, M., Altherr, R., Matthews, A., 1987. Evolution of the Cycladic crystalline complex: petrology,
1108 isotope geochemistry and geochronology, in: *Chemical Transport in Metasomatic Processes*. Springer,
1109 pp. 389–428.
- 1110 Schliestedt, M., Matthews, A., 1987. Transformation of blueschist to greenschist-facies rocks as a consequence
1111 of fluid infiltration, Sifnos (Cyclades), Greece. *Contributions to Mineralogy and Petrology* 97, 237–250.
- 1112 Schmädicke, E., Will, T.M., 2003. Pressure–temperature evolution of blueschist-facies rocks from Sifnos,
1113 Greece, and implications for the exhumation of high-pressure rocks in the Central Aegean. *Journal of*
1114 *Metamorphic Geology* 21, 799–811.
- 1115 Schumacher, J.C., Brady, J.B., Cheney, J.T., Tonnsen, R.R., 2008. Glaucofane-bearing marbles on Syros,
1116 Greece. *Journal of Petrology* 49, 1667–1686.
- 1117 Soukis, K., Stöckli, D.F., 2013. Structural and thermochronometric evidence for multi-stage exhumation of
1118 southern Syros, Cycladic islands, Greece. *Tectonophysics* 595, 148–164.

- 1119 Stouraiti, C., Mitropoulos, P., Tarney, J., Barreiro, B., McGrath, A.M., Baltatzis, E., 2010. Geochemistry and
 1120 petrogenesis of late Miocene granitoids, Cyclades, southern Aegean: Nature of source components.
 1121 *Lithos* 114, 337–352.
- 1122 Terry, M. P., Heidelbach, F., 2006. Deformation-enhanced metamorphic reactions and the rheology of high-
 1123 pressure shear zones, Western Gneiss Region, Norway. *Journal of Metamorphic Geology* 24, 3-18.
- 1124 Tomaschek, F., Kennedy, A.K., Villa, I.M., Lagos, M., Ballhaus, C., 2003. Zircon from Syros, Cyclades,
 1125 Greece—recrystallization and mobilization of zircon during high-pressure metamorphism. *Journal of*
 1126 *Petrology* 44, 1977–2002.
- 1127 Trotet, F., Jolivet, L., Vidal, O., 2001a. Tectono-metamorphic evolution of Syros and Sifnos islands (Cyclades,
 1128 Greece). *Tectonophysics* 338, 179–206.
- 1129 Trotet, F., Vidal, O., Jolivet, L., 2001b. Exhumation of Syros and Sifnos metamorphic rocks (Cyclades, Greece).
 1130 New constraints on the PT paths. *European Journal of Mineralogy* 13, 901–902.
- 1131 Van Hinsbergen, D.J.J., Zachariasse, W.J., Wortel, M.J.R., Meulenkamp, J.E., 2005. Underthrusting and
 1132 exhumation: a comparison between the External Hellenides and the “hot” Cycladic and “cold” South
 1133 Aegean core complexes (Greece). *Tectonics* 24.
- 1134 Vanderhaeghe, O., 2004. Structural development of the Naxos migmatite dome. *Geological Society of America*
 1135 *Special Papers* 380, 211–227.
- 1136 Vitale-Brovarone, A., Groppo, C., Hetenyi, G., Compagnoni, R., Malavieille, J., 2011. Coexistence of lawsonite-
 1137 bearing eclogite and blueschist: phase equilibria modelling of Alpine Corsica metabasalts and
 1138 petrological evolution of subducting slabs. *Journal of Metamorphic Geology* 29, 583–600.
- 1139 Wijbrans, J.R., McDougall, I., 1986. $^{40}\text{Ar}/^{39}\text{Ar}$ dating of white micas from an Alpine high-pressure
 1140 metamorphic belt on Naxos (Greece): the resetting of the argon isotopic system. *Contributions to*
 1141 *Mineralogy and Petrology* 93, 187–194.
- 1142 Wijbrans, J.R., Schliestedt, M., York, D., 1990. Single grain argon laser probe dating of phengites from the
 1143 blueschist to greenschist transition on Sifnos (Cyclades, Greece). *Contributions to Mineralogy and*
 1144 *Petrology* 104, 582–593.